Quaternary Science Reviews 344 (2024) 108975

Contents lists available at ScienceDirect

Quaternary Science Reviews

journal homepage: www.elsevier.com/locate/quascirev

Methane emissions from proglacial lakes: A synthesis study directed toward Lake Agassiz

Laura S. Brosius [a,*], Katey M. Walter Anthony [a], Thomas V. Lowell [b], Peter Anthony [a], Jeffery P. Chanton [c], Miriam C. Jones [d], Guido Grosse [e,f], Andy J. Breckenridge [g]

[a] Water and Environmental Research Center, University of Alaska Fairbanks, PO Box 755910, Fairbanks, AK, 99775-5910, USA
[b] Department of Geology, University of Cincinnati, 500 Geology/Physics Building, Cincinnati, OH, 45221-0013, USA
[c] Department of Earth Ocean and Atmospheric Science, Florida State University, 1011 Academic Way, Tallahassee, FL, 32306, USA
[d] U.S. Geological Survey, Florence Bascom National Center, MS 926A, 12201 Sunrise Valley Dr., Reston, VA, 20192, USA
[e] Alfred Wegener Institute Helmholtz Centre for Polar and Marine Research, Telegrafenberg A45, Potsdam, 14473, Germany
[f] University of Potsdam, Institute of Geosciences, Karl-Liebknecht-Str. 24-25, Potsdam, Golm, 14476, Germany
[g] Natural Sciences Department, University of Wisconsin-Superior, PO Box 2000, Superior, WI, 54880, USA

ARTICLE INFO

Handling editor: I Hendy

ABSTRACT

Large proglacial lakes could have been a significant methane source during the last deglaciation. Today, proglacial lakes are small and mostly limited in the northern hemisphere to the margins of ice sheets in Greenland, Alaska, and Canada, but much larger proglacial lakes collectively flooded millions of square kilometers in the northern hemisphere over the last deglacial period. We synthesize new and existing methane flux measurements from modern proglacial lakes in Alaska and Greenland and use these data together with reconstructed lake area and bathymetry, new paleorecords of sediment organic geochemistry, carbon accumulation, and other proxies to broadly constrain the possible deglacial methane dynamics of a single large North American proglacial lake, Lake Agassiz. While large influxes of glaciogenic material contributed to rapid organic carbon burial during initial lakes phases, limited bioavailability of this carbon is suggested by its likely subglacial origin and prior microbial processing. Water depths of >20 m across 37–90% of the lake area facilitating significant oxidation of methane within the water column further limited emissions. Later phases of lake lowering and subsequent re-expansion into shallow aquatic and subaerial environments provided the most significant opportunity for methane production according to our estimates. We found that Lake Agassiz was likely a small source [0.4–2.7 Tg yr^{-1} mean (0.1–9.9 Tg yr^{-1} 95% CI)] of methane during the last deglaciation on par with emissions from modern wildfires. Although poor constraints of past global proglacial lake areas and morphologies currently prevent extrapolation of our results, we suggest that these systems were likely an additional source of methane during the last deglacial transition that require further study.

1. Introduction

Polar ice core records show that atmospheric methane concentrations (AMC) nearly doubled over the last deglacial transition (Brook et al., 2000). Two abrupt increases, 14.7 thousand years ago (ka) cal BP and 11.6 cal ka BP, were separated by a sharp decrease in concentration synchronous with cooling in the northern hemisphere during the Younger Dryas (12.9–11.6 cal ka BP). While tropical sources dominated global atmospheric methane dynamics, boreal sources may have contributed up to 25 Tg CH_4 yr^{-1} to abrupt AMC increases (Riddell-Young et al., 2023). Recent studies show that northern lake and peatland emissions which increased steadily throughout the deglacial period cannot explain these abrupt changes (Treat et al., 2021; Brosius et al., 2023). Fossil methane sources are also unlikely to have driven abrupt increases in AMC based on the contemporary radiocarbon ages of methane trapped in polar ice cores across these transitions (Petrenko et al., 2017; Dyonisius et al., 2020). This suggests greater importance of a younger methane source that has yet to be determined. Extralimital peatlands that colonized exposed continental shelves (Kleinen et al., 2022; Jones et al., 2023) and portions of the American Midwest (Byun et al., 2021) were recently advanced as a northern source of young carbon contributing to AMC during the last deglaciation. We here

* Corresponding author.
E-mail address: lsbrosius@alaska.edu (L.S. Brosius).

https://doi.org/10.1016/j.quascirev.2024.108975
Received 12 April 2024; Received in revised form 28 August 2024; Accepted 15 September 2024
Available online 29 September 2024

explore the formation of large proglacial lakes during deglaciation as another potential methane source that until now has not been considered in AMC reconstructions.

Proglacial lakes form when meltwater is impounded by glacial margins. While today's proglacial lakes are small (0.05–130 km^2 in Greenland; How et al., 2021), large proglacial lakes flooded several million square kilometers in North America, Europe and Siberia during the last deglaciation (Carrivick and Tweed, 2013). Here we investigate the hypothesis that inundation of large land areas, resulting in the creation of extensive, anaerobic lake-bottom environments, could have facilitated methane production, given adequate organic carbon (OC) sources.

The global relevance of carbon cycling linked directly to ice sheets and glaciers is increasingly recognized. Large organic matter reservoirs and gas hydrates are assumed to be present in subglacial deposits; the ice itself serves as a sink for particulate organic carbon and in situ carbon assimilation at the ice surface (e.g. by ice algae); and modern outlet streams show evidence of elevated methane concentrations and export of partially highly reactive carbon compounds (Wadham et al., 2019). So far, however, the organic geochemistry of glacial sediments has rarely been a topic of interest in proglacial lake studies, which typically focus on sedimentological changes useful for reconstructing ice sheet dynamics. Hence, we take advantage of existing lake cores containing long glaciolacustrine sediment sequences to quantify sediment carbon concentrations and analyze carbon accumulation rates based on varve chronologies.

While proglacial lake formation took place at a global scale, we limit our investigation to the context of a single large North American proglacial lake, Lake Agassiz. At its maximum extent prior to drainage ~8.4 ka BP (all ages calibrated unless otherwise noted), Lake Agassiz occupied 1.5×10^6 km^2 (Teller and Leverington, 2004), and over its lifespan, covered significant portions of present-day Manitoba, Minnesota, North Dakota, Ontario, Quebec, and Saskatchewan. This lake formed in a sub-boreal climate regime surrounded by a combination of cool mixed forest and parkland (Williams et al., 2004; Fastovich et al., 2020), which at various stages was inundated by the lake as it underwent dynamic morphological changes over its ~6000-year history (Teller, 1987).

The primary goal of this study is to explore potential rates of methane emissions from Lake Agassiz using reconstructions of the lake's area and bathymetry, a new depth-flux model derived from observations of methane emissions in present day proglacial lakes, and by comparison to other proxy systems. New paleorecords of sediment organic geochemistry during different stages of inundation allow further exploration of methane dynamics related to organic matter quantity and lability. Modern proglacial lakes are a relatively rare landscape feature today, limited to the perimeters of remaining ice masses. Since very few data

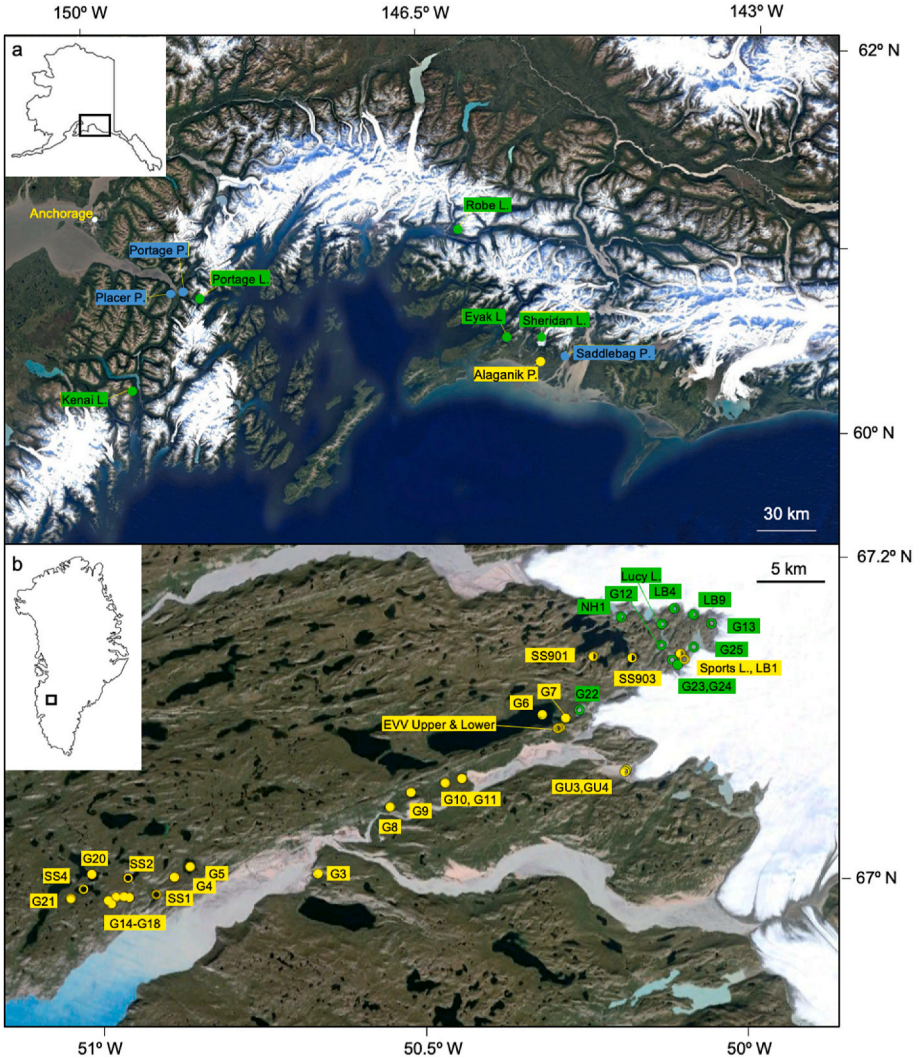

Fig. 1. Study lake locations. Study lakes in Southcentral Alaska (a) and near Kangerlussuaq Greenland (b). Emissions data was collected either by field study (filled circles) or remote sensing (half-filled circles) methods, or a combination of both (open circles) from proglacial lakes (green), glacial lakes (yellow) or proglacial fluvial/isostatic rebound ponds (blue).

exist for methane emissions from modern proglacial lakes, a supporting goal of this study is to synthesize new and existing present-day data for these systems. Our effort to broadly constrain possible methane emissions from one of the larger, more extensive proglacial lakes of the past sheds light on the potential importance of these once widespread features on AMC dynamics during the last deglaciation.

2. Methods

2.1. Proglacial lake methane flux measurements

Little methane emissions data exists for modern proglacial lakes, which are potential analogs for proglacial lake systems of the past. To address this gap, we conducted new field work, compiled data from previous field work, and expanded relationships between field-measured methane fluxes and remote-sensing detection of ebullition seeps to build a database of lake methane fluxes in the glacial regions of Southcentral Alaska (29 lakes) and Kangerlussuaq Greenland (37 lakes) (Fig. 1). Lakes were classified as *proglacial lakes* if they were hydrologically connected to the glaciers on the present-day landscape and as *glacial lakes* if they were hydrologically isolated from the glaciers (Fig. S1). Turbid lakes were assumed to be hydrologically-connected proglacial lakes since glacial meltwater is the source of turbidity in the periglacial landscape. Relatively clear lakes were assumed to be hydrologically isolated glacial lakes. *Proglacial fluvial ponds* were small water bodies adjacent to outflow streams of proglacial lakes.

In Southcentral Alaska, we measured ebullition, diffusive and plant-mediated fluxes in a variety of proglacial and glacial lakes, and ponds formed either in the fluvial drainages of proglacial lakes and/or by ground subsidence associated with isostatic rebound following deglaciation. Diffusive and plant-mediated fluxes were measured using a portable floating chamber method (Elder et al., 2020) whereby a Los Gatos Micro-Portable Greenhouse Gas Analyzer (ABB INC., Quebec City, CA) measured the concentrations of CH_4, CO_2, and water vapor at 1Hz in air that was recirculated through a 6.3-L custom built, semi-transparent, closed chamber and connective Teflon tubing. Floating chamber measurements (n = 3 to 17 spatial replicates per lake) were made only once during the open water season in August 2023. Diffusive fluxes were calculated from the ideal gas law using chamber volume, temperature, and atmospheric pressure. The slope of linear CH_4 concentration change ($R^2 > 0.90$ correlation to linear least squares fit) for a minimum of 45 s (45 observations) and a maximum of 210 s ($45<n>210$) was used to determine mass change within the chambers. Observations with stepwise concentration increases (interpreted as ebullition) were omitted to ensure that the reported measurements represent purely diffusive fluxes. Diffusive emissions were upscaled to an annual estimate assuming observed fluxes represented the open water season for the Southcentral Alaska region (191 days) per Sepulveda-Jauregui et al. (2015).

Ebullition fluxes were measured using submerged bubble traps installed beneath the lake's surface in summer (or below lake ice in winter; Walter Anthony et al., 2012) at locations where point-source seeps occurred as ice-trapped bubbles (i.e. small seeps, Fig. 2b) or as bubbling-induced open holes (Fig. 2a). Gas samples collected from bubble traps into glass serum bottles with butyl rubber septa were analyzed for methane concentration, stable isotopes and radiocarbon ages following Walter Anthony et al. (2012). Briefly, gas bubble concentrations were determined using a Shimadzu gas chromatograph 8A equipped with a thermal conductivity detector, and $\delta^{13}C_{CH4}$ and δD_{CH4}

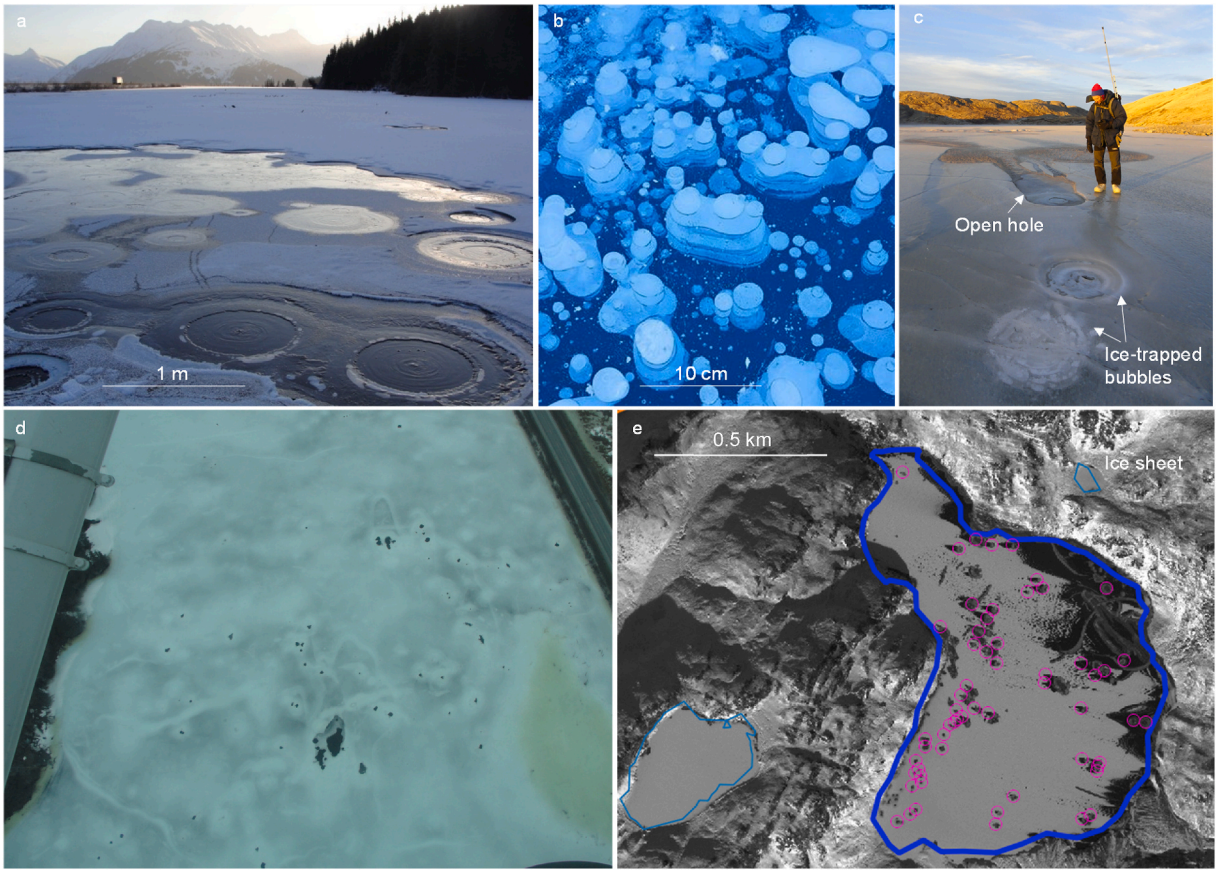

Fig. 2. Images of methane seeps in proglacial lakes. a) Ground photo of open holes in Southcentral Alaska lake ice caused by continuous methane bubbling. b) Ice-trapped bubbles in Portage Lake, Alaska. c) Methane ebullition bubbles trapped in lake ice and bubbling-induced ice-free holes in Greenland. d) Aerial photo of ebullition-induced open holes in winter lake ice Southcentral Alaska (note: Seward Highway on right for scale). e) Magenta circles indicate potential seeps identified as ice-free holes in the October 10, 2011 WorldView-1 image of lake G23 in Greenland.

were determined on a Thermo-Finnegan Delta V isotope ratio mass spectrometer. Precision for these analyses are 0.3‰ and 1.0‰, respectively. For radiocarbon, methane was combusted in a He stream over 800 °C cuprox, then purified cryogenically and sent to the Woods Hole Oceanographic Institution's National Ocean Sciences Accelerator Mass Spectrometer (NOSAMS) facility or the W. M. Keck Carbon Cycle AMS (KCCAMS) Laboratory at UC Irvine for AMS analysis.

In Southcentral Alaska, we calculated annual volumetric ebullition rates for smaller seeps (those identified as ice-trapped bubbles in early winter lake ice) using seep densities (number of seeps per m^2) through fieldwork ice-bubble survey transects (Walter et al., 2007; Walter Anthony et al., 2012; Sepulveda-Jauregui et al., 2015) coupled to associated annual ebullition rates determined through bubble-trap fluxes measured over the short term (1–6 days) at the Southcentral Alaska lakes and year-round on similar small ebullition seeps in other lakes (≈213,000 individual ebullition flux measurements made using submerged bubble traps on 162 seeps in 24 panarctic lakes; Walter Anthony and Anthony, 2013). We converted volumetric ebullition to mass-based estimates of methane ebullition using measured bubble methane concentrations in the Southcentral Alaska region (55 ± 13% by volume, mean ± s.e.m, n = 5). Uncertainties associated with our field-based ebullition estimates for small seep ebullition were calculated for the 95% confidence level by propagating spatial errors associated with ice-bubble surveys, which are a function of survey area and ebullition seep density, and spatiotemporal errors associated seep-class-specific bubble-trap flux measurements (Walter Anthony and Anthony, 2013).

We estimated ebullition fluxes for large seeps (open holes in ice) using the Southcentral Alaska regional mean volumetric ebullition rates associated with the point-source bubble streams that generate the open holes (73 ± 32, L $seep^{-1}$ d^{-1}, mean ± s.e.m, n = 10; Walter Anthony et al., 2012), site-specific bubble methane concentrations (70–91% CH_4 by volume), and the density of seeps, which was the quotient of the number of ebullition-induced open holes counted in aerial photographs and/or ground-based surveys divided by the area surveyed. We calculated the uncertainty associated with the estimated fluxes by propagating errors of seep volumetric flux (43%, relative standard error, RSE), number of seeps per site (10%), errors on surveyed area from combining oblique aerial photos and Google Earth (20%–30% depending on the site), and methane concentration in bubbles (15%).

In Greenland, we utilized existing ebullition data from field work on 25 proglacial and glacial lakes along a transect from Kangerlussuaq, Greenland to the Russell Glacier in October 2010 (Fig. 1) (Walter Anthony et al., 2012). We upscaled field-measured short-term bubble trap fluxes, transect-level ice-bubble seep surveys, and bubble methane concentrations (57 ± 6 % by volume, mean ± s.e.m, n = 8) from Greenland fieldwork to annual ebullition following the same methods and assumptions described for Southcentral Alaska.

To expand our investigation of large (open-hole) seeps in Greenland beyond the previous field studied lakes, we built upon the optical remote sensing approach of Walter Anthony et al. (2012) and Engram and Walter Anthony (2024) to identify large ebullition seeps as open holes in the ice in a combination of field-studied lakes and lakes lacking field data. First, we manually inspected 114 high resolution (0.5 m) optical images from Geoeye1, WorldView-1, and WorldView-2 obtained from the Polar Geospatial Center (PGC) at the locations of 17 known open-hole methane seeps during the early winter ice-cover season from years 2011 through 2020. Because holes created by ebullition seeps are not always discernible in optical images due to darkness, cloud cover, thin ice, and/or snow masking the holes, we selected three satellite images (from among the best 15) in which the field-observed open holes were clearly visible in our Kangerlusuuaq, Greenland area of interest (Fig. S2). Within these images we quantified the number of open holes in 20 lakes selected based on prior field work of ebullition (8 lakes), ancillary field data about lake sediments and/or water chemistry (8 lakes), and differences in lake turbidity observed in satellite images with no prior field knowledge (2 turbid lakes, 1 clear lake). One additional lake (HN1) was added to the study set based on observations of open holes in the imagrey. We counted the number of open holes discerneable within each lake following a Standard Independent Analysis method (Supplementary Methods 1.2). We estimated ebullition fluxes for large seeps in the Kangerlussuaq region by applying volumetric ebullition rates associated with the field-measured bubble streams that generated open holes in Greenland (66 ± 36, L $seep^{-1}$ d^{-1}, mean ± s.e.m, n = 4; Walter Anthony et al., 2012) and bubble methane concentrations (69 ± 6% CH_4 by volume) to the density of open holes determined from satellite imagery and/or ground-based surveys. We calculated the uncertainty associated with the estimated fluxes by propagating errors associated with seep volumetric flux (54% RSE), number seeps per site (10%), methane concentration in bubbles (9%), and errors on surveyed area (10%).

While our estimates of Greenland lake methane emissions account for both smaller ebullition seeps (expressed as ice-trapped bubbles in early winter) and large seeps (expressed as open holes in early winter), we do not include plant-mediated fluxes from Greenland lakes due to a lack of field measurements; however, we expect that in our Greenland study region, plant-mediated fluxes are negligeable since floating-leaf and emergent aquatic vegetation were rarely observed in our 2010 fieldwork.

Finally, to compare methane ebullition to carbon accumulation rates in lake sediments, we report annual ebullition on a lake-by-lake basis. While annual rates of small-seep ebullition derive from year-round monitoring of ebullition with bubble traps (Walter Anthony and Anthony, 2013), no year-round monitoring of ebullition on the large open-hole seeps exists. Therefore, we assumed that our short-term bubble trap fluxes on the large seeps represented ebullition 365 days per year from these seeps. This assumption likely has little impact on our conclusions since short-term fluxes from small seeps were not significantly different from long-term (year-round) fluxes (Walter Anthony and Anthony, 2013) and variability in short-term fluxes observed among individual large seeps was large, varying by two orders of magnigude.

2.2. Lake Agassiz sediment sampling and analysis

To assess the potential for Lake Agassiz sediments to generate microbial methane, we analyzed Lake Agassiz samples from six long (up to 20 m) sediment cores. The cores were retrieved from extant lakes in northern Minnesota and northwestern Ontario between 2015 and 2019 (Breckenridge et al., 2020, 2023, Fig. 3), and are archived at the University of Minnesota Continental Scientific Drilling facility. We subsampled the cores volumetrically to determine dry bulk density (n = 85). We also sampled entire strata (annual varve couplets or multi-year sequences) within cores for geochemical analyses (n = 143). While we did not sample in replicate, we did sample sedimentological units of interest at more frequent intervals with the aim of capturing potential variations in OM sources and origins. Following acidification using muriatic acid (31.45% HCl) and five times rinsing with deionized water, we measured total organic carbon, total organic nitrogen, $\delta^{13}C$, and $\delta^{15}N$ using an elemental analyzer (Finnigan DeltaPlus XP, Thermo Scientific) coupled to a Costech ECS4010 Elemental Analyzer (Costech Scientific, Valencia, California, USA) at the University of Alaska Stable Isotope Facility in Fairbanks, Alaska. Measurement of an internal laboratory standard (peptone) indicated a measurement precision of ≤0.4‰ for C and N isotopes. Sediment organic C and N contents are reported in dry weight percentage (wt %). Stable isotope concentrations are reported in parts per mil (‰). All stable isotope values are expressed relative to Vienna Pe Dee Belemnite (VPDB) and ambient air, respectively. We report all results in mean ± standard deviation (SD). Sample ages are based on the varve chronology, which are placed on an absolute time scale using the radiocarbon ages of transported terrestrial macrofossils within a distinctive isochronous layer (Breckenridge et al., 2020).

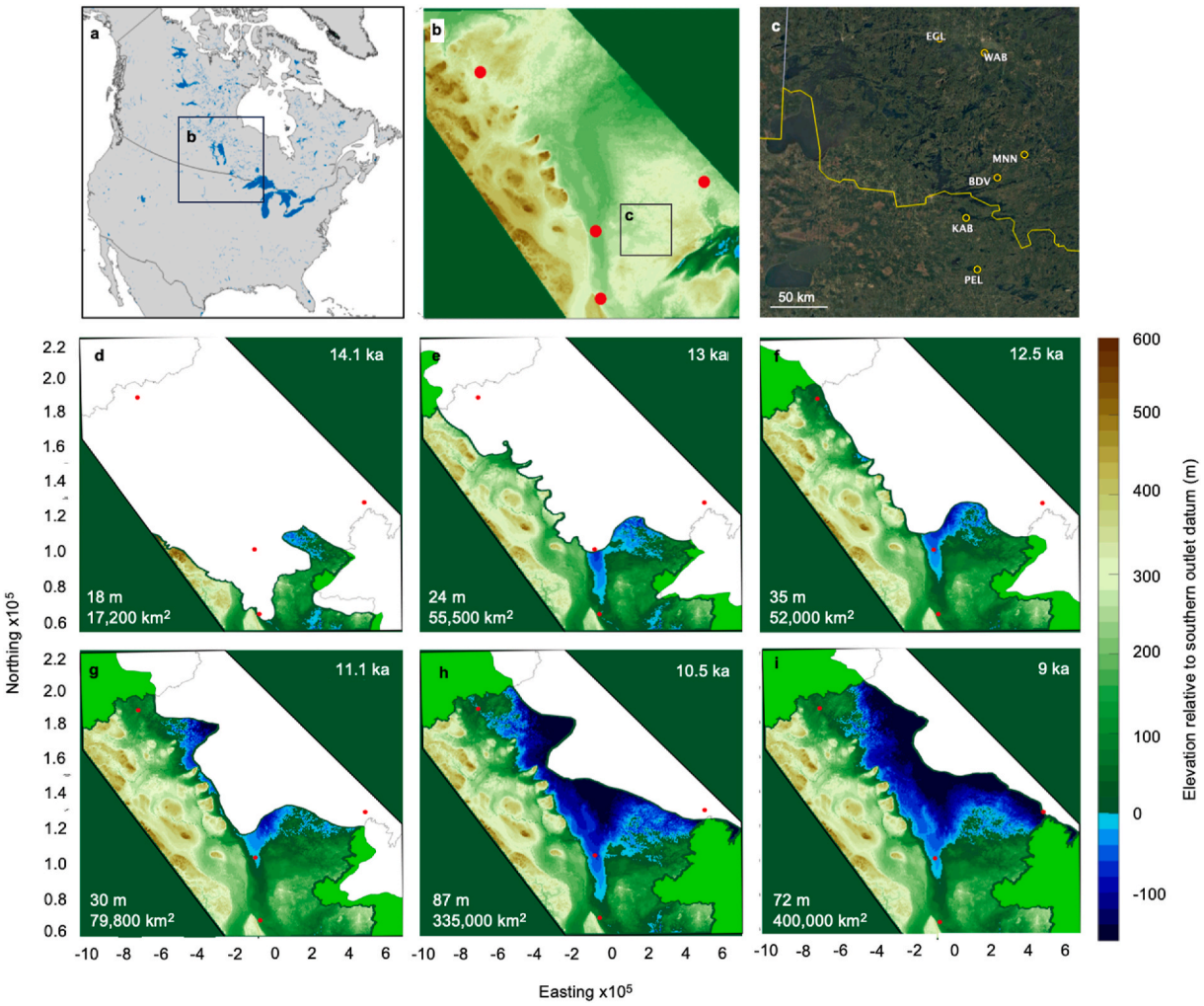

Fig. 3. Lake Agassiz core locations and reconstructed lake areas. General location (a) and present-day topography of the Lake Agassiz region (b). The red dots reference the various low passes in the topography where known or suggested outlets occurred. The center dot is the location of a minimum value of the water level during the Moorhead low from Arndt (1977) (Supplementary Methods 1.1). Locations of lake cores analyzed (yellow circles) in this study are from the eastern part of the lake (c). Reconstructions of Lake Agassiz are shown for six timesteps (d–i), with the ice sheet (white), topography, and continental divides delineating alternate catchment boundaries (green) shown. Negative elevation values indicate inundated areas. Lake areas and mean depths at each timestep are also given.

2.3. Sediment carbon calculations and contextualization

Building upon the work of Breckenridge (2015), Lewis et al. (2022), and Fisher and Breckenridge (2022), we present our geochemical analyses within the context of reconstructed depths and areas of glacial Lake Agassiz at six different points in its roughly 6000-year history (Supplementary Methods 1.1). Briefly, glacial Lake Agassiz flooded a vast lowland created by isostatic depression of the northward-dipping Hudson Bay and Arctic Ocean basins (Teller, 1987), and experienced large changes in depth and area over numerous evolutionary phases between ~14.5 and 8.4 ka BP (Teller and Leverington, 2004).

The lake first established south of the retreating Laurentide Ice Sheet (LIS), filling the headwater valley of what is now the Red River and adjacent basins to the north (Fig. 3d). With continued retreat of the ice sheet, the lake continued to deepen and expand until the Moorhead lake phase at around 12.5 ka BP, when water levels decreased (Fig. 3e and f). Dropping lake levels caused the southern lake margin to retreat northward, while the lake continued to expand along the receding ice front. The timing of the resulting Moorhead low is disputed, and may have been characterized by multiple phases, but the lowest phase is roughly constrained to 12.4–11.5 ka BP (Fisher et al., 2008; Young et al., 2021). Following the Moorhead Low, water levels again rose, and expansion resumed, culminating in the Early Campbell high stand (335,000 km^2, 10.5 ka BP, Fig. 3h), which occurred during the Emerson Phase. The Emerson Phase eventually gave way to farther northward expansion (Fig. 3i), and later coalescence with glacial Lake Ojibway (not reconstructed here) during the final stages of the lake prior to its drainage into Hudson Bay at ~8.4 ka BP.

Utilizing varve thickness measurements for the six cores analyzed for carbon dynamics in this study, we calculated organic carbon accumulation rates (OCARs) for Lake Agassiz sediments. Where sedimentation occurred as indistinct rhythmites or unstratified bulk clays, we applied a linear age-depth model based on bracketing varve years. We calculated 10-year mean OCARs within varved sequences, and sedimentary unit average OCARs within unstratified sediments. Organic carbon fractions of three bulk sediment samples were radiocarbon dated by AMS at the NOSAMS facility to establish a timeframe for unconstrained facies transitions. Radiocarbon ages were calibrated using CALIB 8.2 (Stuiver and Reimer, 1993).

2.4. Statistics

Prior to using analysis of variance (ANOVA), we checked that our data (untransformed or rank-transformed), met standard assumptions, and tests were run using an alpha level of 0.05 unless otherwise specified. If data did not meet the assumptions, we used alternative, non-

parametric statistical tests. We performed a two-sample Kolmogorov Smirnov test to test for differences in the distributions of present-day lake fluxes methane by mode (diffusion vs. total ebullition) among all the study lakes. To compare fluxes for glacial lakes in Alaska vs. Greenland by mode, we used a Type III ANOVA on rank-transformed data. We used linear regression to analyze the relationship between mean water depth at the sampling locations and observed ebullition at both the whole-lake scale and individual-seep scale. For the individual-seep scale flux relationship to water depth, we tested for significant differences in slope between seasons of flux observation. Statistical analyses were performed in R version 4.2.2, using packages car, ggplot2, and MASS.

3. Results & discussion

3.1. Modern proglacial lake methane emissions

3.1.1. Fluxes

As in most freshwater lakes (Kuhn et al., 2021), ebullition exceeded diffusion as the dominant emission mode in our study lakes (Two--Sample Kolmogorov Smirnov D = 0.37, p = .02) (Table 1). Among glacial lakes in Alaska and Greenland, the only lake type for which all emission modes were represented (small and large ebullition seeps together representing total ebullition, and diffusion; Table 1, Fig. 4a), two-way ANOVA revealed no significant interaction between region and emission mode with regard to methane flux ($F(1,37) = 0.18$, $p = .67$), but simple main effects showed that emissions from Southcentral Alaska glacial lakes were higher than from Greenland glacial lakes ($p = .002$).

Known controls over methane emissions from lakes help explain variations in fluxes observed in this study. Prior research has shown that water depth impacts methane emissions in a variety of ways. First, hydrostatic pressure reduces the probability of bubble formation and emission at depths >8 m by around 90% (Bastviken et al., 2004; West et al., 2016). This likely contributed to the negative correlation between mean water depth at the sampling locations and observed ebullition across our study sites (Fig. 5a). This relationship, which becomes asymptotic, also indicated a lack of significant methane ebullition at depths >20 m. Second, deep water enhances dissolution and subsequent oxidation of methane during bubble ascent, with bubbles 10 mm in diameter released at 50-m depth modeled to reach the water surface devoid of methane (McGinnis et al., 2006). The deepest site at which we sampled ebullition seeps was ~25 m at Kenai Lake. While the bubble methane concentration was lower (70%) here than in shallower (1.2–3.7 m) glacial and proglacial lake sites in the same Southcentral Alaska region (79–91%), water depth did not have a negative effect on ebullition at the scale of individual seeps even when bubble methane concentrations were accounted for (Fig. 5b, grey regression line). This was still true when we excluded the more uncertain fluxes measured from a drifting boat in summer open water conditions (Fig. 5b, black regression line). The higher fluxes measured in summer likely represent a bias in our selection of prominent seeps, which were easier to sample from a drifting boat than the adjacent weaker bubble streams. Boat drift also leads to less accurate flux measurements. Regardless of the uncertainties, our results show that within relatively shallow areas (<25 m) of our glacial and proglacial study lakes, bubbles from ebullition seeps reach the atmosphere. Third, substrate availability for methanogenesis is a factor that contributes to the relationship between lake water depth and ebullition. Littoral sediments, which are typically shallower than lake centers, produce and emit more methane than pelagic zones due to higher nutrient loading and organic carbon inputs from algae and plant biomass (Juutinen et al., 2003; Bastviken et al., 2004). Finally, plant mediated fluxes which bypass oxidation are also a component of emissions from shallow littoral zones, which in our study exceeded both ebullition and diffusion where emergent plants were present (Table 1).

While proglacial lakes in Southcentral Alaska tended to be deep (up to 190 m) due to their positions in steep-sided glacial valleys, our sampling locations in these lakes were comparably shallow to typical proglacial lake water depths near Kangerlussuaq, Greenland (<30 m; Burpee et al., 2018). Thus, differences in substrate quantity and bioavailability, rather than water depth, likely explain some of the remaining variation in our field observations. Higher methane emissions from glacial lakes in Alaska compared to Greenland ($p = .002$) may result from a warmer climate (MAAT Valdez, AK: 3.0 °C, MAAT Kangerlussuaq, Greenland: −3.9 °C) and higher ecosystem productivity. Sporadic permafrost, higher terrain relief and more developed drainage systems in Southcentral Alaska also likely facilitate inputs of terrestrial material to glacial lakes, which serve as an additional OC source. This occurs to a much lesser extent in Greenland, where limited hydrological linkage between glacial lakes and their catchments causes autochthonous (primarily algal) OM sources to dominate within sediments (Anderson et al., 2009; Lindborg et al., 2020). This autochthonous OM is subject to aerobic mineralization within glacial lakes, where sediment accumulates slowly (0.27–1.2 mm yr^{-1}, Sobek et al., 2014). However, rapidly buried OM retaining a significant fraction of its reactive carbon component is known to support high rates of methanogenesis (DelSontro et al., 2010; Sobek et al., 2012; Maeck et al., 2013). Our data show that Greenland lakes receiving glacial meltwater inputs (i.e. proglacial lakes) exhibit higher rates of methane bubbling than those which are hydrologically disconnected from the ice sheet (i.e. glacial lakes, Table 1), possibly due to the preservation of labile substrates by rapidly deposited glacial sediments.

By far the highest emissions in our study were from strong ebullition seeps occurring in very shallow (1–4 m) ponds that dotted the fluvial outflows of proglacial lakes near Portage, Alaska, and/or which formed as a result of 1.8 m of ground subsidence and inundation in this area

Table 1
Summary of fluxes by mode, lake type and region.

Total seep ebullition		Southcentral Alaska			Kangerlussaq, Greenland	
		Proglacial	Glacial	F/I Ponds	Proglacial	Glacial
				Ebullition ($g\ CH_4\ m^{-2}\ yr^{-1}$)		
		>5 ± 2	24 ± 10	>189 ± 59	45 ± 34	1.2 ± 0.2
Small seeps	mean	nd	24 ± 10	nd	11 ± 4	1.2 ± 0.2
	n sites		*11*		*6*	*20*
Large seeps	mean	5 ± 2	0 ± 0	189 ± 59	34 ± 22	0 ± 0
	n sites	*4*	*2*	*11*	*10*	*27*
				Diffusion ($g\ CH_4\ m^{-2}\ yr^{-1}$)		
	mean	3 ± 1	6 ± 1	12 ± 4	nd	0.6
	n sites	*5*	*9*	*3*		*1*
				Plant-mediated ($g\ CH_4\ m^{-2}\ yr^{-1}$)		
	mean	nd	154 ± 81	206	nd	nd
	n sites		*3*	*1*		

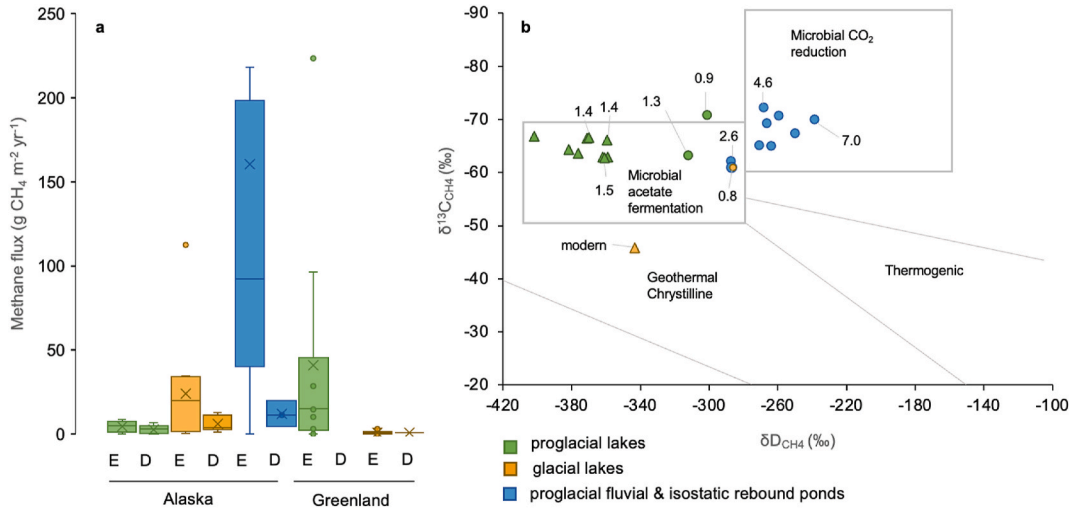

Fig. 4. Methane fluxes and isotope composition. Methane emitted by ebullition (E) or diffusion (D) from proglacial lakes, glacial lakes, and proglacial fluvial/isostatic rebound ponds in Greenland and Alaska (a). Box plots show mean, inner quartile, minimum and maximum values. Median values (x's) and outliers (circles) are also shown. Stable isotope compositions and radiocarbon ages given in ^{14}C ka BP of methane emitted from lakes and ponds in Greenland (triangles) and Alaska (circles) (b). The enriched $^{13}C_{CH4}$ value of the outlier likely resulted from sample oxidation within the trap during bubble accumulation over several days. Panel b is after Whiticar (1999).

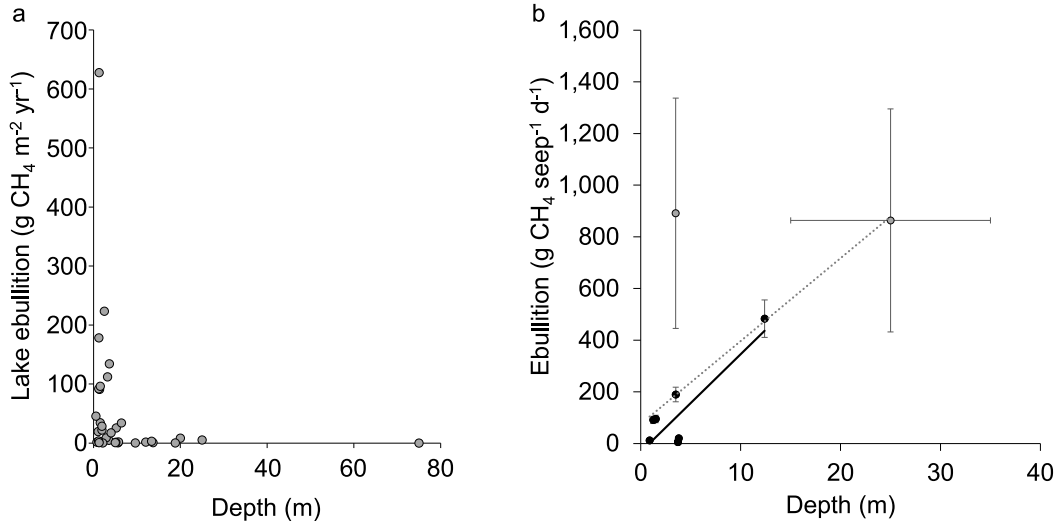

Fig. 5. Methane ebullition as a function of water column depth at the scales of whole-lake surfaces (a) and individual seeps (b). In b, the correlation between mean water depth at sampling locations and ebullition for wintertime observations (black dots and line), when ice provides a stable platform for more accurate measurements, was $y = 32x + 76$ ($r^2 = 0.46$, $F(1,8) = 6.75$, $p = .032$). Excluding the less accurate and biased summer observations (grey dots and line; see main text), the correlation was $y = 38x - 33$ ($r^2 = 0.73$, $F(1,6) = 16.1$, $p = .007$), and the confidence interval for the grey line includes the black line, so the slopes can be considered the same. Errors in panel *b* represent uncertainties based on field-measured volumetric fluxes using submerged bubble traps in winter from a solid ice platform (black dots, ~15%) and summer from a drifting boat (grey dots, ~50%). The relatively large error bar on depth at Kenai Lake (25 ± 10 m, derived from a bathymetric map coupled to GPS points of the measured seep) is due to water depth exceeding our depth sounder and steepness of the lake bottom at this seep's location.

following the 1964 megathrust earthquake in Southcentral Alaska (Plafker, 1969). Located along a tectonically active subsidence zone containing faults prone to earthquakes and surrounded by alpine glaciers and ice fields, the hydrologic setting of our Southcentral Alaska field site is obscured by complex interactions among tectonic forces, isostatic rebound, and eustatic sea-level rise (Reger et al., 2007). Coseismic subsidence events, which appear to occur every ~700–800 years in this area (Combellick, 1994), inundated coastal ecosystems producing "ghost" forests and buried peats deposits (Ovenshine et al., 1976) that may be the source of large amounts of terrestrially derived organic carbon fueling methane production in proglacial fluvial and isostatic rebound ponds (Fig. 4a).

3.1.2. Isotopes

Stable isotope signatures and radiocarbon ages of methane in Alaska and Greenland ebullition samples indicate microbial formation from relatively young organic carbon substrates (Fig. 4b). This contrasts with ebullition fluxes from glacial and proglacial lakes between Cordova and Katalla along the Gulf of Alaska where thermogenic sources have also been documented (Walter Anthony et al., 2012). Both the distribution of $\delta^{13}C_{CH4}$ and δD_{CH4} (Fig. 4b), and apparent fractionation of carbon (α_c) and hydrogen (α_d) during methanogenesis calculated using the equations:

$$\alpha_c = \frac{\alpha_c = \delta\,^{13}C - CO_2 + 1000}{\delta\,^{13}C - CH_4 + 1000} \quad \text{Eq. (1)}$$

$$\alpha_d = \frac{\delta D - H_2O + 1000}{\delta D - CH_4 + 1000} \quad \text{Eq. (2)}$$

and site-specific δD_{H2O} values, suggest dominance of different methanogenic pathways between study locations.

Lower α_c (1.01 ± 0.01) and higher α_d (1.31 ± 0.08) values associated with Greenland lake emissions confirm methane production by acetate fermentation (Fig. 4b) associated with the decomposition of more labile substrates (Hornibrook et al., 1997) such as algal biomass, despite the potential influence of extremely D-depleted proglacial lake water (−145 to −217‰; Cluett and Thomas, 2020; Henkemans et al., 2018) on δD_{CH4} (Chanton et al., 2006), and are consistent with previous isotope measurements from a glacial lake in the Kangerlussuaq area (Thompson et al., 2016). Interestingly, methane is produced via the same pathway in both glacial and proglacial lakes in this area, despite differences in bubble ^{14}C-CH_4 age (modern and 1.4 ^{14}C ka BP, respectively). Production of methane from buried organic-rich facies of non-glacial origin dating to the mid-Holocene, when glaciers were absent from proglacial lake catchments in this area (e.g. Lucy Lake; Young & Briner, 2015), could explain this finding. However, more research is necessary to identify specific OM sources fueling methanogensis in Greenlandic proglacial lakes. Other sources may include contemporary carbon fixed within the lake or on the ice sheet surface, old subglacial OC and/or aeolian inputs of terrestrial OM (Anderson et al., 2017).

In the Alaskan proglacial fluvial/isostatic rebound ponds, which exhibited comparatively higher α_c (1.04 ± 0.02) values, lower α_d (1.21 ± 0.04) values, and older radiocarbon ages of evolved methane, CO_2 reduction dominated as the primary production pathway. Methane formation from older and more recalcitrant sources of OCpresent in large quantities, such as buried peats or other terrestrial OM suspected to fuel methane production in these locations, is consistent with these results (Hornibrook et al., 1997), and lends further support to the conclusion that OC quantity and quality, in addition to water depth, contribute to variations in methane fluxes from modern glacial-region lakes.

3.2. Extrapolating modern analog methane fluxes to estimate emissions from Lake Agassiz

In order to extrapolate methane flux observations from present-day proglacial lake systems to Lake Agassiz, it is first necessary to understand the limnological context and relevance of the ancient lake system. In section 3.3, we provide this context through our analysis of lake core stratigraphy, sediment organic carbon accumulation rates and geochemistry. In section 3.4 we discuss observations of these sediment characteristics and implications for supporting methane production and emissions throughout different phases of Lake Agassiz' evolution from 14 to 11 ka BP. Finally, in Section 3.5 we present emission estimates from Lake Agassiz throughout the deglacial period based on the modern analog systems.

3.3. Lake Agassiz sediment characteristics

3.3.1. Generalized core stratigraphy

Lake cores analyzed in this study were principally composed of thick (up to 20 m) rapidly deposited 0.74 (0.47–1.33) cm yr^{-1} [median (inner quartile range)] glaciogenic sediments. Differences in the sequence and timing of major stratigraphic units amongst the six cores sampled reflect the complex morphological history of Lake Agassiz and its interactions with the Laurentide Ice Sheet (Fig. S3). We distinguished three general sedimentary units (Fig. 6) representative of different depositional environments clearly dictated by ice sheet proximity, and less distinctly by changes in water depth and lake morphometry: ice-proximal sediments (Fig. 6a), ice-distal sediments (Fig. 6b and c) and unstratified sediments (Fig. 6e). A fourth unit (Fig. 6d), representative of three anomalous "thick varve events" is not expressly considered within this study.

Ice-proximal Sediments: Ice-proximal varved sediments are annual

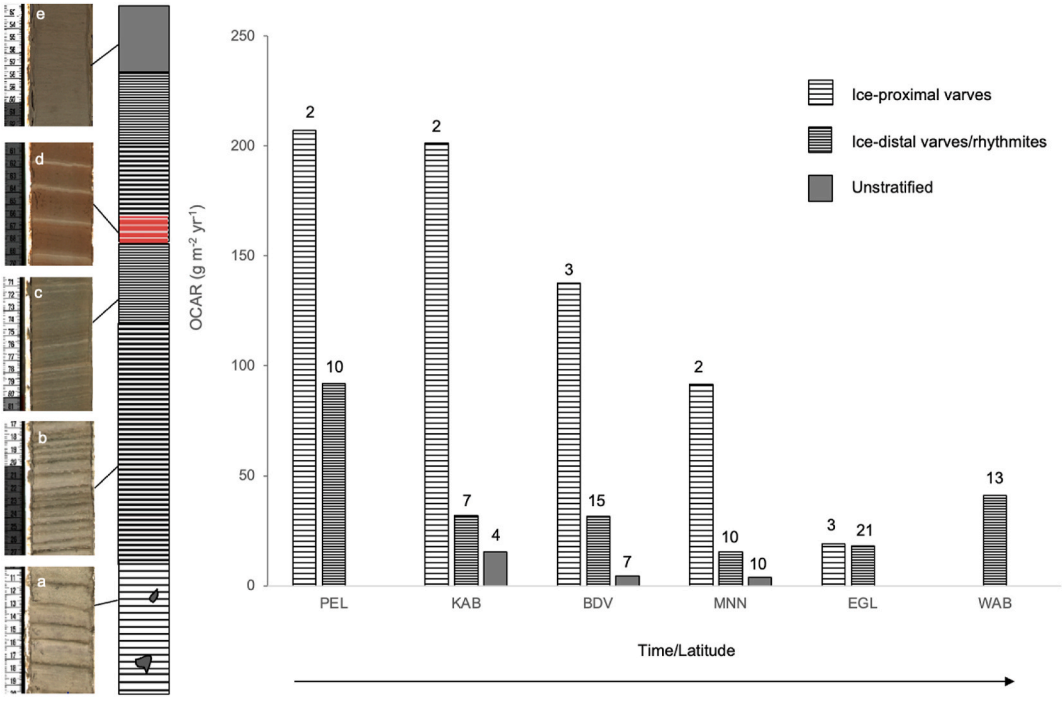

Fig. 6. Sedimentary units and their organic carbon accumulation rates. Generalized stratigraphy of Lake Agassiz sediment cores with representative photographs of ice-proximal varves (note centimeter marks on ruler for scale) (a), ice-distal varves (b), rhythmites (c), thick red varves (d) and unstratified/massive clays (e). Bar graph shows mean organic carbon accumulation rates and n data points for each sedimentary unit and sampling location (Fig. 3). Ice-proximal varves from WAB were present but not sampled.

couplets composed of courser-grained and lighter-colored melt-season bands, capped by darker, finer-grained bands deposited during winter, ice-covered conditions (Rittenhouse, 1933; Antevs, 1951; Breckenridge et al., 2020). The ice-proximal zones of Lake Agassiz accumulated thicker couplets produced by high-density meltwater undercurrents near the ice front, whereas the clay caps resulted from suspension settling, perhaps following mixing of the lake and widespread dispersal. As reported in other large, proglacial lakes, ice-proximal melt season layers can be internally complex, and composed of multiple silty or sandy laminae that may be graded (Ridge et al., 2012). Faster sedimentation and inputs of ice-rafted debris in these ice-proximal environments are indicated by thick varves and clasts present in the lowermost sediment sequences (Fig. 6a). In the selection of six cores from the southern subbasins of Lake Agassiz on which we focus this study (Fig. 3), ice-proximal sediment sequences averaged ~1 m thick and accumulated at a rate of 1.48 (0.87–2.77) cm yr^{-1} (Breckenridge et al., 2020, 2023). The organic carbon concentrations of ice-proximal units were 0.43 ± 0.30%.

Ice-distal Sediments: Overlying thick ice-proximal varves, are longer sequences of thinly varved or indistinctly stratified glacial clays (rhythmites; Fig. 6b and c) that accumulated at a rate of 0.49 (0.27–0.91) cm yr^{-1} (Breckenridge et al., 2020, 2023). These sediments had similarly low organic carbon concentrations (0.39 ± 0.22%) and were likely formed by slower sedimentation processes in more ice-distal locations, where warm surface water inflows contribute to thermal stratification, and effect water currents responsible for sediment distribution (Ashley, 1975). Ice-distal varves were distinguished from ice-proximal varves by a decrease in the rate of varve thickness change to <0.25 cm yr^{-1} based on a polynomial curve fit to the data. Three anomalous thick varve events deposited around 12.5, 12.3 and 11.5 ka BP punctuate each of the core records spanning this timeframe. While distinctive red clays transported from >100 km away by drainage of proglacial Lake Kaministiquia compose the final thick "red varve" unit at 11.5 ka BP (Breckenridge et al., 2020, Fig. 6d), the two prior thick varve events remain unexplained.

Unstratified Sediments: Sequences of unstratified/massive clay sediments deposited 12.1 ka BP or later (Fig. 6e) and containing 0.22 ± 0.19% OC provide preliminary evidence for climate- and ice sheet-driven changes in lake morphology, including lake lowering and potential isolation of smaller, internal basins during the well-documented Moorhead Low (Fisher et al., 2008). Average sedimentation rates for these units are an order of magnitude lower (0.17 ± 0.04 cm yr^{-1}) than those for ice-proximal units.

3.3.2. Sediment organic carbon accumulation rates

Average OCARs in ice-proximal (131 g C m^{-2} yr^{-1}) and ice-distal (38 g C m^{-2} yr^{-1}) zones of Lake Agassiz were similar to those reported other proglacial lake systems: proglacial Lake Superior (8–120 g C m^{-2} yr^{-1} in the Duluth and Caribou subbasins; up to 600 g C m^{-2} yr^{-1} in the Thunder Bay trough; Hyodo and Longstaffe, 2011); and 25–140 g C m^{-2} yr^{-1} for a modern proglacial lake during periods of glacial meltwater influx (Larsen et al., 2011). Unstratified unit OCARs (Fig. 6) averaging 7 g C m^{-2} yr^{-1} fell within the range of long-term mean OCARs reported for glacial lakes in western Greenland (6 g C m^{-2} yr^{-1}; Anderson et al., 2009), boreal Quebec (3.8 g C m^{-2} yr^{-1}; Ferland et al., 2012), and across Europe (5.6 C g m^{-2} yr^{-1}; Kastowski et al., 2011). All OCARs were strongly correlated with sedimentation rates (Fig. 7, Fig. S4); and OCARs for each sedimentary unit decreased between cores spanning a gradient of both time and latitude (Fig. 6).

3.3.3. Sediment organic geochemistry

Sediment organic C and N concentrations, C/N ratios and $\delta^{13}C$ signatures in proglacial Lake Agassiz were similar to those in proglacial Lake Superior (Hyodo and Longstaffe, 2011, Fig. S5), which also received large amounts of glaciogenic material from the retreating Laurentide Ice Sheet prior to 8.8 ka BP. Though few studies have analyzed the organic matter contents of modern proglacial lake sediments of glaciogenic origin, these are also characterized by low OC concentrations (<1%) (Adamson et al., 2019; Larsen et al., 2011), C/N ratios of 10–14 (Larsen et al., 2011) and $\delta^{13}C$ values of around −26‰ during periods of meltwater influx (Young and Briner, 2015).

Regression analyses revealed significant changes in sediment organic geochemistry from lake initiation (~14 ka BP) until ~12.5 ka BP, over which time total sediment organic matter C and N concentrations

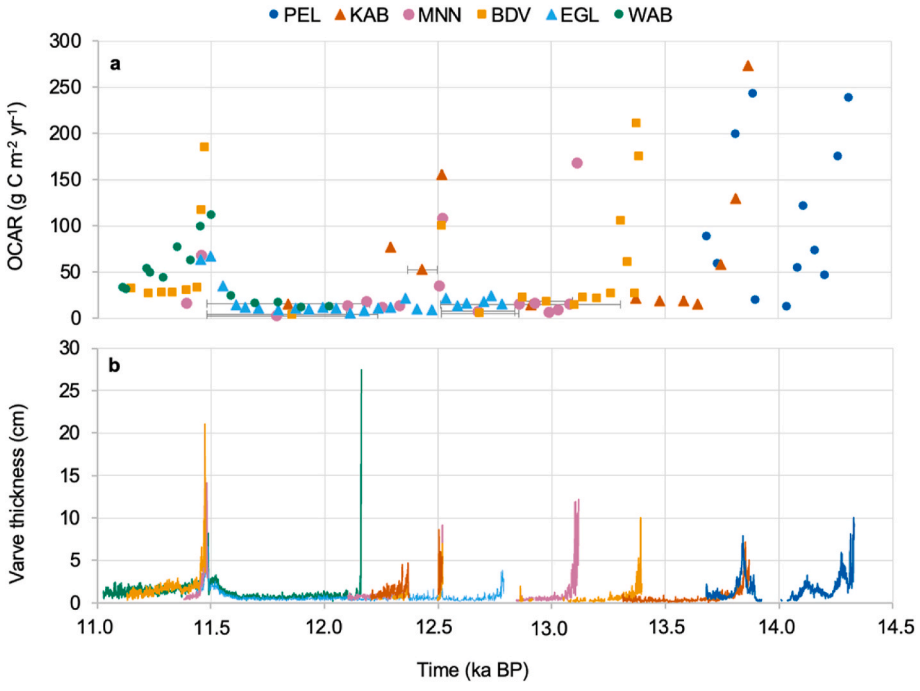

Fig. 7. Carbon and sediment accumulation rates. Organic carbon accumulation rates (a), and varve thicknesses (b) indicative of annual sedimentation rates in our six study lakes. Varve thicknesses and chronologies are from Breckenridge et al. (2020, 2023).

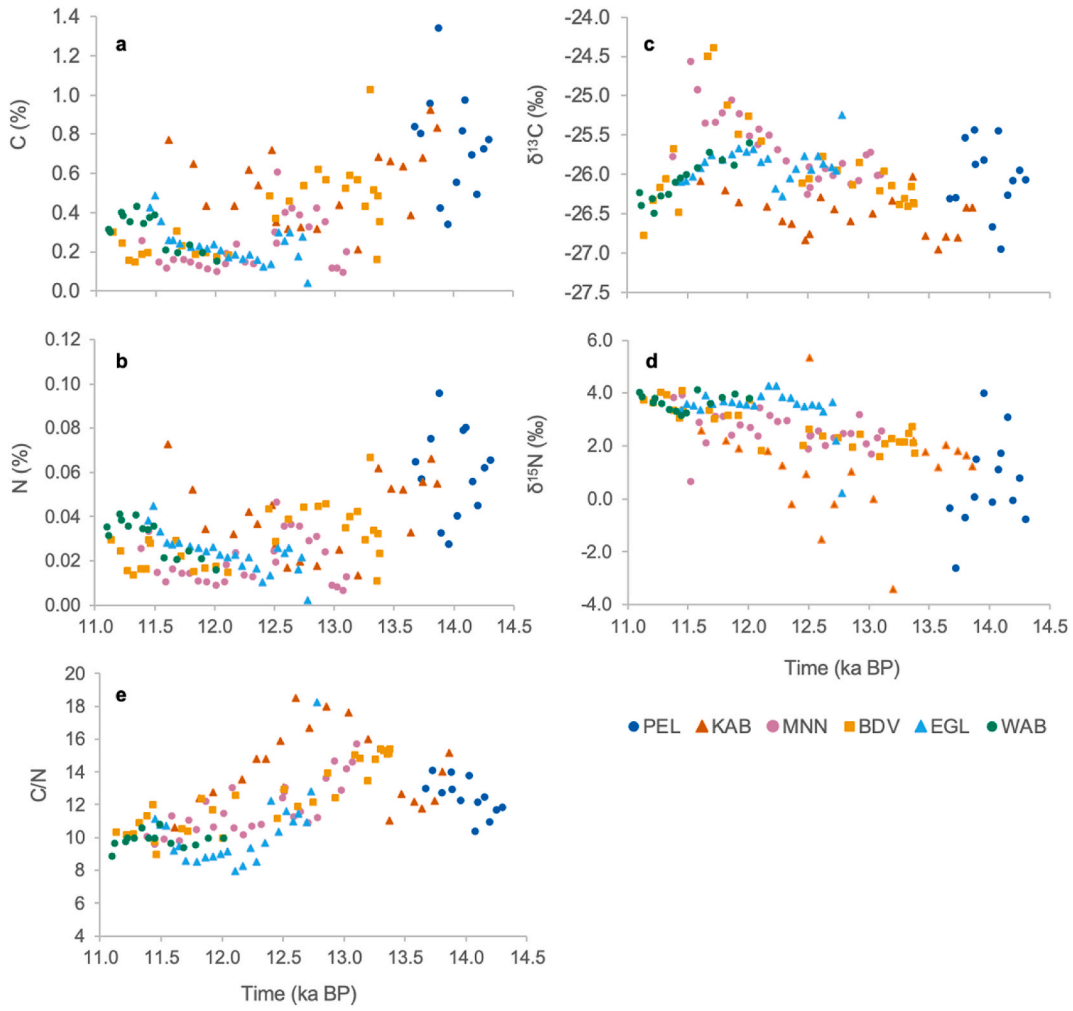

Fig. 8. Temporal trends in sediment organic matter characteristics. Organic carbon (a), nitrogen (b), $\delta^{13}C$ (c), $\delta^{15}N$ (d) concentrations and C/N ratios (e) of organic matter in glacial Lake Agassiz sediments over time color-coded by coring site; n = 133.

decreased and became more enriched in $\delta^{13}C$ and $\delta^{15}N$ (Fig. 8a–d, $p<0.02$). After 12.5 ka BP, C and N concentrations increased, but the direction of trends in C/N, $\delta^{13}C$ and $\delta^{15}N$ remained mostly constant (Fig. 8). A sharp decrease in $\delta^{13}C$ at some sites (MNN, BDV, KAB) after ~11.5 ka BP was not accompanied by a clear change in any of the other metrics (Fig. 8). AMS analysis of bulk organic carbon from two glacial sediment samples yielded ages of 18.1 and 38.1 ka BP (Fig. S3, Table S1). Three data points from the thick "red varve" event at 11.5 ka were excluded from Figs. 6 and 8, and statistical analyses due a clear difference in sediment providence.

3.4. *Organic carbon sources and implications for methane dynamics of Lake Agassiz*

Extremely large proglacial lakes are unique to past deglacial phases where massive ice sheets supplied large volumes of meltwater. To provide a first assessment of deglacial methane emissions from a single large proglacial lake, Lake Agassiz, we applied depth-dependent fluxes observed in modern analog systems to reconstructions of this lake's area and bathymetry, treating drained and reflooded lake areas separately due to the unique establishment of terrestrial ecosystems in these locations (Supplementary Methods 1.3). Since in addition to water depth, both OM quantity (related to primary productivity) and bioavailability exert control over methane emissions (Juutinen et al., 2003; Bastviken et al., 2004), new records of Lake Agassiz organic carbon accumulation and sediment organic matter geochemistry allow independent validation of our approach by comparison to modern-day lakes in which rates of long-term sediment organic carbon accumulation influence methane emissions (Fig. 9), and inform discussion of potential methane dynamics within Lake Agassiz at different phases of its evolution.

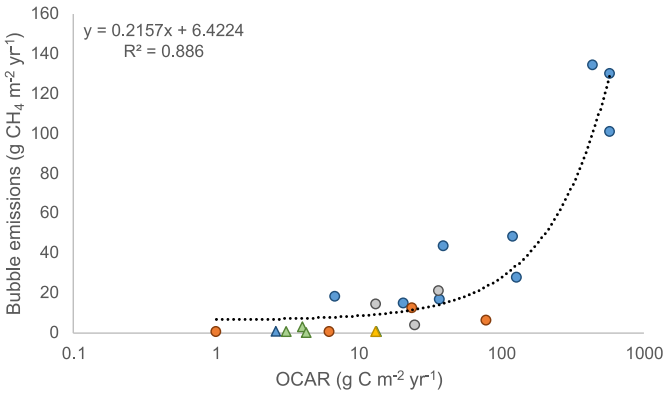

Fig. 9. Relationship between OCAR (organic carbon accumulation rate) and bubble methane emissions. Data are from thermokarst lakes (circles) and glacial lakes (triangles) in Greenland (green), Sweden (yellow), northern Siberia (orange), interior Alaska (blue) and northwest Alaska (grey) (Table S2).

Table 2
Lake Agassiz morphological dynamics and associated methane emission estimates. Reconstructed depths and areas of Lake Agassiz, associated morphological dynamics, and estimated methane emissions at each timestep [mean (95% CI)].

Time (ka BP)	Mean depth (m)	Lake (km^2)	Lake <20 m (km^2)	Drained Lake (km^2)	Reflooded Drained Basin (km^2)	Upland (km^2)	Methane emissions (Tg yr^{-1})
14.1	18	17,200	10,781	–	–	–	0.4 (0.1–2.9)
13.0	24	55,500	28,350	1800	–	–	1.0 (0.3–7.8)
12.5	35	52,000	18,025	37,975	–	–	0.7 (0.2–5.1)
11.1	30	79,800	27,158	28,975	–	–	1.1 (0.3–8.2)
10.5	87	335,000	48,947	–	53,375	50,400	2.7 (0.8–9.9)
9.0	72	400,000	39,823	81,750	14,400	–	2.1 (0.6–9.0)

3.4.1. Early phases of lake expansion (14–12.5ka BP)

During its earliest phases, 35–63% of Lake Agassiz was <20 m deep (Table 2) and therefore likely to support methane emissions. Early lake phases were also characterized by low sediment OC concentrations (0.41 ± 0.36%), and high rates of sedimentation (0.74 cm yr^{-1}) and associated carbon accumulation (up to ~200 g C m^{-2} yr^{-1}, Fig. 6) that resulted from large influxes of glaciogenic material and efficient OC burial due to limited oxygen exposure (<0.1 yr for burial efficiencies >80% associated with sedimentation rates >0.2 cm yr^{-1} in modern systems; Sobek et al., 2009). Lake Agassiz OCARs during this time (Fig. 6) were comparable to those in thermokarst lakes receiving large inputs of retransported terrestrial material generated by permafrost thaw and shoreline slumping (132 ± 201 g C m^{-2} yr^{-1}, Table S2); and OCARs of this magnitude could have supported methane emissions of up to 52 g CH_4 m^{-2} yr^{-1} (Fig. 9).

Despite apparently adequate substrate volumes, rates of methane production were also likely dependent on the lability of the sediment organic carbon pool, which was in turn determined by its origin and degree of prior decomposition. Lake Agassiz $\delta^{13}C$ and $\delta^{15}N$ signatures and C/N ratios for sediments older than 12.5 ka BP predominantly fall within the range of values reported for mineral soil and subglacial sediment OM that has been subject to some degree of microbial processing (Fig. S5, Dümig et al., 2012; Mainka et al., 2022, Vinšová et al., 2022). While geochemical imprinting by these processes renders these sources virtually indistinguishable from other microbial sources (e.g. phytoplankton and benthic algae), Lake Agassiz glacial sediment OM most likely originated from the subglacial/supraglacial environment during its earliest phases due to limitation of aquatic primary productivity by low water temperature and high turbidity. This limitation is demonstrated in Lake Agassiz by the absence of silicacious microfossils in ice-proximal glaciogenic strata (Risberg et al., 1999; Teller et al., 2008). Prior studies have likewise advanced a subglacial origin of geochemically similar OM (Fig. S5) contained in proglacial Lake Superior sediments (Hyodo and Longstaffe, 2011) and young glacial foreland soils (Dümig et al., 2012; Khedim et al., 2021). Bulk sediment OC ages of 18.1 and 38.1 ka BP provide further evidence for the incorporation of OM that was pre-aged compared to its time of deposition (Table S1).

Lake Agassiz sediment OM became enriched in heavy stable isotopes (^{13}C, ^{15}N; Fig. 8) from lake inception until ~12.5 ka BP. Sedimentary unit OCARs also decreased coincident with ice sheet retreat (Fig. 6). We interpret this to imply a gradual reduction in sediment OM loading from subglacial/supraglacial sources, and a simultaneous shift toward progressively older and/or more reworked OC originating from deeper within the ice sheet (Kohler et al., 2017). This explanation accounts for observed trends in $\delta^{13}C$, $\delta^{15}N$ and C/N, which are consistent with the microbial transformation of old subglacial OC (Dümig et al., 2012; Vinšová et al., 2022) and deep mineral soils (Mainka et al., 2022) during which accumulating microbial biomass becomes part of the mineral aggregate, thereby modifying its organic geochemistry.

The importance of subglacial OM as a carbon source to proglacial lake methane production is largely unknown. As ice sheets expanded during the last glaciation, they bulldozed and buried previously existing ecosystems, resulting in the entrainment of organic carbon into basal ice and subglacial sediments (Punkari and Forsström, 1995; Wadham et al. 2008, 2019). In modern proglacial environments, radiocarbon-depleted POC and DOC originating from a mixture of modern supraglacial and old subglacial sources, are found in glacial meltwater streams (Bhatia et al., 2010, 2013; Hood et al., 2009), which export an estimated 6 Tg C yr^{-1} from global ice sheets (Wadham et al., 2019). Where lakes are hydrologically connected to glaciers, this DOC/POC is deposited into the lake basin (Bhatia et al., 2013; Osburn et al., 2017). While no prior study has specifically quantified lacustrine deposition of subglacial DOC/POC, it is likely that some of the 418–610 Pg OC buried beneath the Laurentide Ice Sheet at the LGM (Wadham et al., 2008) became incorporated into proglacial lake sediments during the last deglaciation.

Several lines of evidence suggest that subglacial OM can fuel methane production. These include incubations of debris-rich basal ice and subglacial sediments (Skidmore et al., 2000; Stibal et al., 2012), and observations of glacial meltwater streams supersaturated in methane that has originated from supra/subglacial carbon sources (Burns et al., 2018; Lamarche-Gagnon et al., 2019). High concentrations of dissolved methane in some confined groundwater aquifers have also been attributed to in situ decomposition of organic matter buried during the last glaciation in both North America and Europe (Aravena et al., 1995; Raidla et al., 2019). Though subglacial OM typically lacks readily available carbon substrates due to a high degree of prior microbial processing (Skidmore et al., 2000; Bardgett et al., 2007; Vinšová et al., 2022), the potential for remobilization of this slow carbon pool by methanogenesis, even after thousands of years, is potentially evidenced by ^{14}C-depleted ages of methane produced in modern proglacial lakes (0.9–7.0 ^{14}C ka BP, Fig. 4b). Evolution of methane from incubated Lake Agassiz glacial clay soils with an age of 20 ^{14}C ka BP commenced only after extended lag times (hundreds of days) and proceeded very slowly (0.1 mol% d^{-1}) or sometimes not at all (Sheppard et al., 1996, 1997), suggesting that old subglacial OC was likely a major, but fairly stable component of total sediment OC in proglacial lakes. This gradual mineralization of recalcitrant OM contrasts with high rates of methane production in thermokarst lakes, where recently thawed, and significantly more labile permafrost carbon stocks (van Dongen et al., 2008) become depleted within a few centuries (Walter Anthony et al., 2021).

We posit that shallow portions of Lake Agassiz during its earliest phases may have exhibited methane dynamics similar to those in modern proglacial lakes in Greenland on the basis of relatively shallow depth. However, Lake Agassiz at this time may have been unique compared to modern systems. On one hand, its position in a temperate/sub-boreal climate zone implies potentially higher primary productivity in the terrestrial ecosystem surrounding Lake Agassiz compared to present-day Greenland. On the other hand, geochemical data imply that the Lake Agassiz sediment carbon pool was composed primarily of potentially refractory subglacial OM, which could reduce rates of methanogenesis relative to modern analogs where sediment OM sources fueling methanogenesis are so far unknown. Further study of modern proglacial lake sediment composition, as well as detailed analyses of subglacial soil OM quality in relation to methane production (e.g. Heslop et al., 2017) would better inform comparison of these modern and ancient systems.

3.4.2. Northward expansion and lake lowering during the Moorhead phase (12.5–11.4 ka BP)

Substantial evidence exists for the establishment of shallow lake,

wetland and terrestrial environments during low water stages of the Moorhead phase when at least 68,750 km^2 of the former lake was drained (Fig. 3, Table 2). Organic-rich facies, vegetation changes indicated by pollen and macrofossils, and shifting diatom assemblages in Lake Agassiz sediments suggest that a range of environments from shallow pools (Ashley, 1975) and lagoons (Teller et al., 2000), to peatlands (Fisher et al., 2008; Björck and Keister, 1983; Bajc et al., 2000, Teller et al., 2008; Boyd, 2007), marshlands, and forested ridges (Yansa and Ashworth, 2005) developed during this time. The resulting environment was likely similar in composition to the open, wet, no-analog parkland biome distinguished by the presence of *Fraxinus, Picea* and *Larix* spp. that dominated the Midwest during deglaciation (Fastovich et al., 2020; Byun et al., 2021).

Despite evidence for the development of subaerial environments in some portions of the Agassiz basin, our coring sites appear to have remained submerged based on an absence of terrestrial macrofossils. A partial reversal of earlier trends in sediment organic geochemistry after ~12.5 ka BP (Fig. 8) also suggests a shift toward more bioavailable contemporary sediment carbon sources around the time of lake lowering during the Moorhead phase (Fig. 3). A decrease in C/N ratios toward those typical of lacustrine algae (<10), slowly increasing C and N concentrations, and increasing stable isotope values are consistent with those changes expected to result from an increase in aquatic primary productivity. Such an increase likely occurred as meltwater contributions subsided with retreat of the LIS and/or lake lowering that may have reduced or temporarily isolated at least three of our coring sites (MNN, BDV, KAB) from meltwater influence. Evidence for isolation of these sites includes the onset of unstratified sedimentation (Fig. S3) and a decrease in OCAR (7 g C m^{-2} yr^{-1}, Fig. 6) toward the long-term means for glacial lakes in Europe (5.6 g m^{-2} yr^{-1}, Kastowski et al., 2011) and Greenland (6 g m^{-2} yr^{-1}, Anderson et al., 2009). A rapid increase in $\delta^{13}C$ observed in these records between 12.4 and 11.5 ka BP (Fig. 8) could have resulted from attendant decreases in turbidity and increases in water temperature and productivity that decreased dissolved CO_2 concentrations, thereby reducing discrimination against uptake of isotopically heavier CO_2. Cessation of calcareous glacial sediment inputs, which caused the dissolution of ostracod shells within this portion of the record (Breckenridge, *personal communication*), may also be implicated in these changes.

On land, vegetation succession and soil building over timescales of decades to centuries following ice retreat likely increased terrestrial carbon stocks and may have enhanced opportunities for carbon remobilization (Harden et al., 1992; Khedim et al., 2021; Hodkinson et al., 2003; Juselius et al., 2022; Bradley-Cook and Virginia, 2018). However, an increase in terrestrial OM contributions with C/N ratios and $\delta^{15}N$ values typical of land plants (>20 and ~0.5‰, respectively; Meyers and Ishiwatari, 1993) would have generated trends in opposition to those observed and is not suggested by the data for our sampling sites.

Based on the environmental changes described above, we suggest that the portions of Lake Agassiz which were isolated from meltwater influence during the Moorhead may have been more similar to modern glacial lakes in Greenland, in which labile autochthonous OM sources also dominate (Anderson et al., 2009), than in Alaska, where terrestrial inputs likely play a larger role.

3.4.3. Lake transgression and further northward expansion (11.4–8.5 ka BP)

Subsequent transgression of Lake Agassiz to the Upper Campbell Level (335,000 km^2 at 10.5 ka, Fig. 3, Table 2) inundated shallow aquatic and terrestrial ecosystems that established during the Moorhead, which would have become an immediate carbon source for methane production. Our reconstruction shows that 41% of total lake expansion from 11.1 to 10.5 ka (104,000 km^2) was into upland or drained lake areas. Further expansion until 9 ka inundated an additional 14,400 km^2 of drained lake area (Table 2). Although total flooded carbon stocks are unknown, their anaerobic decomposition likely resulted in methane dynamics similar to those observed with hydroelectric reservoir creation, or formation of Alaskan ponds following sudden ground subsidence (Section 3.1.1). We observed high emissions (>189 g CH_4 m^2 yr^{-1}, Table 1) from the Alaskan ponds >50 years after their formation (Fig. 4a), likely due to inundation of the former terrestrial ecosystem. Similarly, short-term (5–10 year) methane pulses followed by elevated emissions relative to those measured pre-flooding have been attributed to decomposition of the labile carbon pool in terrestrial soils and vegetation flooded by reservoir filling (Kelly et al., 1997; Teodoru et al., 2012). This suggests that a similar pulse in methane release may have resulted from the flooding of terrestrial ecosystems by transgressive expansion of Lake Agassiz during the early Holocene. Such a pulse response may not have been an isolated event. Numerous smaller lake level fluctuations suggested by previous reconstructions (Teller and Leverington, 2004) may have elicited a similar response.

At our study sites, resumed deposition of varved glacial sediments after 11.4 ka BP implies reconnection of sites that were isolated from meltwater influence during the Moorhead low (BDV, MNN, KAB). A decrease in sediment $\delta^{13}C$ at these sites beginning around this time could be attributed to lake water cooling (despite warming early Holocene air temperatures) following reconnection with Lake Agassiz. A temperature-driven increase in dissolved CO_2 concentrations could explain observed decreases in $\delta^{13}C$ due to increased plant and algal discrimination against isotopically heavier CO_2. Alternatively, changes in the isotopic composition of the dissolved inorganic carbon pool may have been caused the reintroduction of calcareous glacial sediments.

Continued northward expansion of Lake Agassiz into areas that were heavily depressed by isostatic forces due to their position more internal to the former ice sheet resulted in the formation of extensive deep lake areas during the later Emerson Phase (Fig. 3). Reconstructions indicate that after 10.5 ka BP, substantial methane emissions were therefore limited to transgressively flooded and shallow (<20 m) lake areas representing a small fraction (10–15%) of total lake area (Table 2).

3.5. Emission estimates from Lake Agassiz based on modern analog systems

Table 2 presents our estimates of methane emissions from Lake Agassiz during its different developmental phases based on applying depth-dependent fluxes observed in modern analog systems to reconstructions of Agassiz' area and bathymetry, and by treating drained and reflooded lake areas separately due to the unique establishment of terrestrial ecosystems in these locations (Supplementary Methods 1.3).

Our findings suggest that Lake Agassiz emitted a maximum of 2.7 (95% CI: 0.8–9.9) Tg CH_4 yr^{-1} during phases of transgressive lake growth that inundated shallow aquatic and terrestrial environments; however, the lake emitted less than 1.1 (95% CI: 0.2–8.1) Tg CH_4 yr^{-1} during the remainder of its lifespan (Table 2). These emissions are comparable to those from global wildfires today (1–5 Tg CH_4 yr^{-1}; Kirschke et al., 2013). Our estimates account for the strong influence of large differences in water depth on ebullition fluxes, but do not directly address the effect of changing OM quantities, sources and bioavailability across gradients of space and time as discussed above.

Higher methane fluxes from small lakes and ponds located in glaciated regions of Alaska (Fig. 4a–Table 1) suggest that our emission estimates for Lake Agassiz may be conservative at the landscape scale. Extensive wetlands, littoral zones and isolated water bodies produced by the lake's fluctuating water levels and complex shorelines may have emitted more methane on a per area basis. However, to avoid double counting, we did not estimate emissions from these features, which may be included in other lake and wetland inventories. It is important to note that while these environments may have been spatially accounted for in previous deglacial wetland assessments (Byun et al., 2021), unique high-flux seeps which our data suggest were present in these areas have not been represented. Given the lack of data about the extent of peripheral fluvial ponds and wetlands that could have been emitting

methane produced in underlying proglacial lake sediments, we did not attempt to estimate the magnitude of this source. However, the large fluxes associated with these environments would have disproportionately increased the region's proglacial methane emissions.

Finally, geologic methane is known to escape from some proglacial aquatic environments in Alaska, Norway, and Greenland (Walter Anthony et al., 2012; Reynolds et al., 2017; Kleinen et al., 2022); however, the absence of hydrocarbon reservoirs beneath former Lake Agassiz (Hackley and Cardott, 2016) suggests this source was unlikely for this location during the last deglaciation. Our estimates represent a first effort to explore and quantify methane emissions from a single ancient proglacial lake. A better understanding of modern proglacial lake methane dynamics, as well as expanded and refined proglacial lake records, characterization of glacial sediment OM, and lake area reconstructions are required to improve upon this work.

3.6. Implications for global proglacial lakes

We synthesized new and existing data sets on modern proglacial lake methane dynamics and focused our reconstruction of paleo-proglacial lake emissions on a single ancient proglacial lake, the maximum extent of which was 1,500,000 km^2 prior its drainage at 8.4 ka (Teller and Leverington, 2004). Lake Agassiz methane dynamics likely differed from other major proglacial lake systems whose specific interactions with regional topography, climate, and ice sheet dynamics contributed to their unique sedimentological, morphological and lake water level histories. Many ancient proglacial lakes were fed by large northward flowing river systems draining the Eurasian continent that delivered additional POC and DOC from the contemporary environment, for example. Others experienced repeated cycles of catastrophic drainage and refilling (e.g. Lake Missoula; Waitt, 1980). Although poor constraints of past global proglacial lake areas and morphologies currently prevent extrapolation of our results, these systems are estimated to have occupied an additional one to two million square kilometers (Mangerud et al., 2001; Lyså et al., 2010; Komatsu et al., 2016) and were likely an additional source of methane that should be further studied. A better understanding of proglacial lake methane dynamics is important in light of expected increases in proglacial lake extents with climate warming (Tweed and Carrivick, 2015).

4. Conclusion

New paleorecords show that large influxes of glaciogenic material from the Laurentide Ice Sheet contributed to rapid organic carbon burial within Lake Agassiz during its initial phases, and within glacially influenced zones of the lake throughout its history (Fig. 6). The geochemical signature of OM in these sediments suggests a high degree of prior microbial processing, however, that calls into question the bioavailability of this potential organic carbon source and may preclude high rates of methane production during early lake stages. Methane dynamics associated with transgressive lake phases may have differed substantially from those of earlier lake phases. Significant lake expansion occurred into upland or previously drained lake areas colonized by shallow aquatic or terrestrial vegetation during the early Holocene (Table 2). Although total flooded carbon stocks are unknown, their anaerobic decomposition could have resulted in methane dynamics akin those observed following hydroelectric reservoir creation. Utilizing reconstructions of Lake Agassiz' area and bathymetry and leveraging present day fluxes from glacial and proglacial lakes and hydrologic reservoirs that serve as end-member proxies to broadly constrain possible methane emissions, we found that Lake Agassiz was likely a small source (0.4–2.7 Tg yr^{-1}) of methane during the last deglaciation.

Funding sources

This work was funded by NSFP2C2 grant 1903735. NSFEAR grants 1602788, 1602789, 1602791 supported the recovery and development of the varve chronology. Grants from the Comer Science and Education Foundation to T. Lowell supported work on Lake Agassiz reconstructions. No funding sources were involved in activities beyond research support.

Data availability

Data produced by this study are publicly archived at https://doi.org/10.6084/m9.figshare.c.7164916. All other supporting data are provided in figures and tables within the manuscript text and supporting materials.

CRediT authorship contribution statement

Laura S. Brosius: Conceptualization, Investigation, Formal analysis, Writing – original draft. **Katey M. Walter Anthony:** Supervision, Conceptualization, Investigation, Writing – original draft, Funding acquisition. **Thomas V. Lowell:** Methodology, Software, Visualization. **Peter Anthony:** Formal analysis. **Jeffery P. Chanton:** Investigation. **Miriam C. Jones:** Conceptualization, Funding acquisition. **Guido Grosse:** Conceptualization, Funding acquisition. **Andy J. Breckenridge:** Investigation, Visualization, Resources, All authors contributed to Writing – Review & Editing.

Declaration of competing interest

The authors declare that they have no known competing financial interests or personal relationships that could have appeared to influence the work reported in this paper.

Data availability

Data produced by this study are publicly archived at doi:10.6084/m9.figshare.c.7164916.

Acknowledgements

We thank Hilary Nystrom and Prajna Lindgren for assistance processing optical imagery, Jorgen Anthony for field work, Guillaume Lamarche-Gagnon for insightful discussion, and the helpful staff at both CSD and ASIF for assistance with lake sediment sampling and analyses.

Appendix A. Supplementary data

Supplementary data to this article can be found online at https://doi.org/10.1016/j.quascirev.2024.108975.

References

Adamson, K., Lane, T., Carney, M., Bishop, T., Delaney, C., 2019. High-resolution proglacial lake records of pre-Little Ice Age glacier advance, northeast Greenland. Boreas 48, 535–550.

Anderson, N.J., D'andrea, W., Fritz, S.C., 2009. Holocene carbon burial by lakes in SW Greenland. Glob. Change Biol. 15, 2590–2598.

Anderson, N.J., et al., 2017. The Arctic in the twenty-first century: changing biogeochemical linkages across a paraglacial landscape of Greenland. Bioscience 67, 118–133.

Antevs, E., 1951. Glacial clays in steep rock lake, Ontario, Canada. Geol. Soc. Am. Bull. 62, 1223–1262.

Aravena, R., Wassenaar, L.I., Plummer, L.N., 1995. Estimating 14C groundwater ages in a methanogenic aquifer. Water Resourc. Res 31, 2307–2317.

Arndt, B.M., 1977. Stratigraphy of Offshore Sediment, Lake Agassiz–North Dakota (Report of Investigation – North Dakota Geological Survey No. 60, Issue.

Ashley, G.M., 1975. Rhythmic sedimentation in glacial lake Hitchcock, Massachusetts-Connecticut. In: Jopling, A.V., McDonald, B.C. (Eds.), Glaciofluvial and Glaciolacustrine Sedimentation, vol. 23. Soc. Econ. Min. Paleont. Spec. Publ., pp. 304–320

Bajc, A.F., Schwert, D.P., Warner, B.G., Williams, N.E., 2000. A reconstruction of Moorhead and Emerson phase environments along the eastern margin of glacial Lake Agassiz, rainy river basin, northwestern Ontario can. J. Earth Sci. 37, 1335–1353.

Bardgett, R.D., et al., 2007. Heterotrophic microbial communities use ancient carbon following glacial retreat. Biol. Lett. 3, 487–490.
Bastviken, D., Cole, J., Pace, M., Tranvik, L., 2004. Methane emissions from lakes: dependence of lake characteristics, two regional assessments, and a global estimate. Global Biogeochem. Cycles 18, GB4009.
Bhatia, M.P., Das, S.B., Longnecker, K., Charette, M.A., Kujawinski, E.B., 2010. Molecular characterization of dissolved organic matter associated with the Greenland ice sheet. Geochim. Cosmochim. Acta 74, 3768–3784.
Bhatia, M.P., Das, S.B., Xu, L., Charette, M.A., Wadham, J.L., Kujawinski, E.B., 2013. Organic carbon export from the Greenland ice sheet. Geochim. Cosmochim. Acta 109, 329–344.
Björck, S., Keister, C.M., 1983. The Emerson phase of Lake Agassiz, independently registered in northwestern Minnesota and northwestern Ontario. Can. J. Earth Sci. 20, 1536–1542.
Breckenridge, A., et al., 2020. A new glacial varve chronology along the southern Laurentide Ice Sheet that spans the Younger Dryas–Holocene boundary. Geology 49, 283–288.
Breckenridge, A., Wattrus, N., Stangeland, Q.A., 2023. The Mid-continent Varve Chronology (Minnesota/Ontario). https://doi.org/10.17605/OSF.IO/J485C.
Breckenridge, A., 2015. The Tintah-Campbell gap and implications for glacial Lake Agassiz drainage during the Younger Dryas cold interval. Quat. Sci. Rev. 117, 124–134.
Brook, E.J., Harder, S., Severinghaus, J., Steig, E.J., Sucher, C.M., 2000. On the origin and timing of rapid changes in atmospheric methane during the last glacial period. Global Biogeochem. Cycles 14, 559–572.
Boyd, M., 2007. Early postglacial history of the southeastern Assiniboine Delta, glacial Lake Agassiz basin. J. Paleolimnol. 37, 313–329.
Bradley-Cook, J.I., Virginia, R.A., 2018. Landscape variation in soil carbon stocks and respiration in an Arctic tundra ecosystem, west Greenland. Arcti. Antarct. Alp. Res 50, S100024.
Brosius, L.S., Walter Anthony, K.M., Treat, C.C., Jones, M.C., Dyonisius, M., Grosse, G., 2023. Panarctic lakes exerted a small positive feedback on early Holocene warming due to deglacial release of methane. Comm. Earth & Environ. 4, 271.
Burns, R., et al., 2018. Direct isotopic evidence of biogenic methane production and efflux from beneath a temperate glacier. Sci. Rep. 8, 17118.
Burpee, B.T., Anderson, D., Saros, J.E., 2018. Assessing ecological effects of glacial meltwater on lakes fed by the Greenland Ice Sheet: the role of nutrient subsidies and turbidity. Arct. Antarc. alp. Res. 50, S100019.
Byun, E., Sato, H., Cowling, S.A., Finkelstein, S.A., 2021. Extensive wetland development in mid-latitude North America during the Bølling–Allerød. Nat. Geosci. 14, 30–35.
Carrivick, J.L., Tweed, F.S., 2013. Proglacial lakes: character, behaviour and geological importance. Quat. Sci. Rev. 78, 34–52.
Chanton, J.P., Fields, D., Hines, M.E., 2006. Controls on the hydrogen isotopic composition of biogenic methane from high-latitude terrestrial wetlands. J. Geophys. Res. 111, G04004.
Cluett, A.A., Thomas, E.K., 2020. Resolving combined influences of inflow and evaporation on western Greenland lake water isotopes to inform paleoclimate inferences. J. Paleolimnol. 63, 251–268.
Combellick, R.A., 1994. Investigation of Peat Stratigraphy in Tidal Marshes along Cook Inlet, Alaska to Determine the Frequency of 1964-style Great Earthquakes in the Anchorage Region, vols. 94–7. Alaska Division of Geological & Geophysical Surveys Report of Investigations, p. 24.
DelSontro, T., McGinnis, D.F., Sobek, S., Ostrovsky, I., Wehrli, B., 2010. Extreme methane emissions from a Swiss hydropower reservoir: contribution from bubbling sediments. Env. Science Technol. 44, 2419–2425.
Dümig, A., Häusler, W., Steffens, M., Kögel-Knabner, I., 2012. Clay fractions from a soil chronosequence after glacier retreat reveal the initial evolution of organo–mineral associations. Geochim. Cosmochim. Acta 85, 1–18.
Dyonisius, M.N., et al., 2020. Old carbon reservoirs were not important in the deglacial methane budget. Science 367, 907–910.
Elder, C.D., Thompson, D.R., Thorpe, A.K., Hanke, P., Walter Anthony, K.M., Miller, C.E., 2020. Airborne mapping reveals emergent power law of arctic methane emissions. Geophys. Res. Lett. 47, e2019GL085707.
Engram, M., Walter Anthony, K., 2024. Synthetic Aperture Radar (SAR) detects large gas seeps in Alaska lakes. Eviron. Res. Lett. 19, 044034.
Fastovich, D., Russell, J.M., Jackson, S.T., Williams, J.W., 2020. Deglacial temperature controls on no-analog community establishment in the Great Lakes Region. Quat. Sci. Rev. 234, 106245.
Fisher, T.G., Breckenridge, A., 2022. Relative lake level reconstructions for glacial lake Agassiz spanning the Herman to Campbell levels. Quat. Sci. Rev. 294, 107760.
Ferland, M.E., del Giorgio, P.A., Teodoru, C., Prairie, Y.T., 2012. Long-term C accumulation and total C stocks in boreal lakes in northern Quebec. Glob. Biogeochem. Cycles 26, GB0E04.
Fisher, T.G., et al., 2008. The chronology, climate, and confusion of the Moorhead phase of glacial Lake Agassiz: new results from the ojata beach, north Dakota, USA. Quat. Sci. Rev. 27, 1124–1135.
Hackley, P.C., Cardott, B.J., 2016. Application of organic petrography in North American shale petroleum systems: a review. Int. J. Coal Geol. 163, 8–51.
Harden, J.W., et al., 1992. Dynamics of soil carbon during deglaciation of the Laurentide ice sheet. Science 258, 1921–1924.
Henkemans, E., Frape, S.K., Ruskeeniemi, T., Anderson, N.J., Hobbs, M., 2018. A landscape-isotopic approach to the geochemical characterization of lakes in the Kangerlussuaq region, west Greenland. Arct. Antarc. alp. Res. 50, S100018.
Heslop, J., Walter Anthony, K., Zhang, M., 2017. Utilizing pyrolysis GC-MS to characterize organic matter quality in relation to methane production in a thermokarst lake sediment core. Org. Geochem. 103, 43–50.
Hodkinson, I.D., Coulson, S.J., Webb, N.R., 2003. Community assembly along proglacial chronosequences in the high Arctic: vegetation and soil development in north-west Svalbard. J. Ecol. 91, 651–663.
Hood, E., et al., 2009. Glaciers as a source of ancient and labile organic matter to the marine environment. Nature 462, 1044–1047.
Hornibrook, E.R., Longstaffe, F.J., Fyfe, W.S., 1997. Spatial distribution of microbial methane production pathways in temperate zone wetland soils: stable carbon and hydrogen isotope evidence. Geochim. Cosmochim. Acta 61, 745–753.
How, P., et al., 2021. Greenland-wide inventory of ice marginal lakes using a multi-method approach. Sci. Rep. 11, 4481.
Hyodo, A., Longstaffe, F.J., 2011. The palaeoproductivity of ancient Lake Superior. Quat. Sci. Rev. 30, 2988–3000.
Jones, M.C., et al., 2023. Past permafrost dynamics can inform future permafrost carbon-climate feedbacks. Comm. Earth. Environ. 4, 272.
Juselius, T., et al., 2022. Newly initiated carbon stock, organic soil accumulation patterns and main driving factors in the High Arctic Svalbard, Norway. Sci. Rep. 12, 4679.
Juutinen, S., et al., 2003. Major implication of the littoral zone for methane release from boreal lakes. Glob. Biogeochem. Cycles 17, 1117.
Kastowski, M., Hinderer, M., Vecsei, A., 2011. Long-term carbon burial in European lakes: analysis and estimate. Glob. Biogeochem. Cycles 25.
Kelly, C.A., et al., 1997. Increases in fluxes of greenhouse gases and methyl mercury following flooding of an experimental reservoir. Env. Sci. Technol. 31, 1334–1344.
Khedim, N., et al., 2021. Topsoil organic matter build-up in glacier forelands around the world. Glob. Change Biol. 27, 1662–1677.
Kirschke, S., et al., 2013. Three decades of global methane sources and sinks. Nat. Geosci. 6, 813–823.
Kohler, T.J., et al., 2017. Carbon dating reveals a seasonal progression in the source of particulate organic carbon exported from the Greenland Ice Sheet. Geophys. Res. Lett. 44, 6209–6217.
Kleinen, T., Gromov, S., Steil, B., Brovkin, V., 2022. Atmospheric methane since the LGM was driven by wetland sources. Clim. Past Discuss 2022, 1–30.
Komatsu, G., et al., 2016. Catastrophic flooding, palaeolakes, and late Quaternary drainage reorganization in northern Eurasia. Int. Geol. Rev. 58, 1693–1722.
Kuhn, M.A., et al., 2021. BAWLD-CH_4 a comprehensive dataset of methane fluxes from boreal and arctic ecosystems. Earth Syst. Sci. Data 13, 5151–5189.
Lamarche-Gagnon, G., et al., 2019. Greenland melt drives continuous export of methane from the ice-sheet bed. Nature 565, 73–77.
Larsen, D.J., Miller, G.H., Geirsdóttir, Á., Thordarson, T., 2011. A 3000-year varved record of glacier activity and climate change from the proglacial lake Hvítárvatn, Iceland. Quat. Sci. Rev. 30, 2715–2731.
Lewis, C.M., Breckenridge, A.J., Teller, J.T., 2022. Reconstruction of isostatically adjusted paleo-strandlines along the southern margin of the Laurentide ice sheet in the great lakes, Lake Agassiz, and champlain sea basins. Can. J. Earth Sci. 59, 826–846.
Lindborg, T., et al., 2020. A carbon mass-balance budget for a periglacial catchment in West Greenland – linking the terrestrial and aquatic systems. Sci. Total Environ. 711, 134561.
Lyså, A., Jensen, M.A., Larsen, E., Fredin, O., Demidov, I.N., 2010. Ice-distal landscape and sediment signatures evidencing damming and drainage of large pro-glacial lakes, northwest Russia. Boreas 40, 481–497.
Maeck, A., et al., 2013. Sediment trapping by dams creates methane emission hot spots. Env. Science Technol. 47, 8130–8137.
Mainka, M., et al., 2022. Soil geochemistry as a driver of soil organic matter composition: insights from a soil chronosequence. Biogeosciences 19, 1675–1689.
Mangerud, J., Astakhov, V., Jakobsson, M., Svendsen, J.I., 2001. Huge Ice-age lakes in Russia. J. Quat. Sci. 16, 773–777.
McGinnis, D.F., Greinert, J., Artemov, Y., Beaubien, S.E., Wüest, A.N.D.A., 2006. Fate of rising methane bubbles in stratified waters: How much methane reaches the atmosphere? J. Geophys. Res.: Oceans 111 (C9).
Meyers, P.A., Ishiwatari, R., 1993. Lacustrine organic geochemistry – an overview of indicators of organic matter sources and diagenesis in lake sediments. Organic Geochem. 20, 867–900.
Osburn, C.L., et al., 2017. Shifts in the source and composition of dissolved organic matter in Southwest Greenland lakes along a regional hydro-climatic gradient. J. Geophys. Res.: Biogeosci. 122, 3431–3445.
Ovenshine, A.T., Lawson, D.E., Bartsch-Winkler, S.R., 1976. The Placer River Silt-intertidal Sedimentation Caused by the Alaska Earthquake of March 27, 1964, vol. 4. U.S. Geological Survey Journal of Research, pp. 151–162.
Petrenko, V.V., et al., 2017. Minimal geological methane emissions during the Younger Dryas–Preboreal abrupt warming event. Nature 548, 443–446.
Plafker, G., 1969. Tectonics of the March 27, 1964 Alaska Earthquake. U.S. Geological Survey Professional Paper 543–I, p. 74.
Punkari, M., Forsström, L., 1995. Organic remains in Finnish subglacial sediments. Quat. Res. 43, 414–425.
Raidla, V., et al., 2019. Origin and formation of methane in groundwater of glacial origin from the Cambrian-Vendian aquifer system in Estonia. Geochim. Cosmochim. Acta 251, 247–264.
Reger, R.D., Sturmann, A.G., Berg, E.E., Burns, P.A.C., 2007. A Guide to the Late Quaternary History of Northern and Western Kenai Peninsula, Alaska. Division of Geological and Geophysical Surveys, Fairbanks.
Riddell-Young, B., et al., 2023. Atmospheric methane variability through the Last Glacial Maximum and deglaciation mainly controlled by tropical sources. Nat. Geosci. 16, 1174–1180.
Ridge, J.C., et al., 2012. The New North American Varve Chronology: a precise record of southeastern Laurentide ice sheet deglaciation and climate, 18.2–12.5 KYR BP, and correlations with Greenland ice core records. Amer. J. Sci. 312, 685–722.

Risberg, J., Sandgren, P., Teller, J.T., Last, W.M., 1999. Siliceous microfossils and mineral magnetic characteristics in a sediment core from Lake Manitoba, Canada: a remnant of glacial Lake Agassiz. Can. J. Earth Sci. 36, 1299–1314.
Rittenhouse, G., 1933. A Study of Varved Clays of Northwestern Ontario [MS Thesis]. University of Chicago, Chicago, p. 29.
Reynolds, P., et al., 2017. Hydrothermal vent complexes offshore Northeast Greenland: a potential role in driving the PETM. Earth Planet Sci. Lett. 67, 72–78.
Sepulveda-Jauregui, A., Walter Anthony, K.M., Martinez-Cruz, K., Greene, S., Thalasso, F., 2015. Methane and carbon dioxide emissions from 40 lakes along a north–south latitudinal transect in Alaska. Biogeosciences 12, 3197–3223.
Sheppard, M.I., Stroes-Gascoyne, S., Hawkins, J.L., Hamon, C.J., Motycka, M., 1996. Methane Production Rates from Natural Organics of Glacial Lake Clay and Granitic Groundwater. Atomic Energy of Canada Limited. Report [11510].
Sheppard, M.I., Stroes-Gascoyne, S., Motycka, M., Hamon, C.J., 1997. The Influence of the Presence of Sulphate on Methanogenesis in the Backfill of a Canadian Nuclear Fuel Waste Disposal Vault: A Laboratory Study. Atomic Energy of Canada Limited. Report [11764].
Skidmore, M.L., Foght, J.M., Sharp, M.J., 2000. Microbial life beneath a high Arctic glacier. Appl. Environ. Microbiol. 66, 3214–3220.
Sobek, S., et al., 2009. Organic carbon burial efficiency in lake sediments controlled by oxygen exposure time and sediment source. Limnol. Oceanog. 54, 2243–2254.
Sobek, S., DelSontro, T., Wongfun, N., Wehrli, B., 2012. Extreme organic carbon burial fuels intense methane bubbling in a temperate reservoir. Geophys. Res. Lett. 39.
Sobek, S., Anderson, N.J., Bernasconi, S.M., Del Sontro, T., 2014. Low organic carbon burial efficiency in arctic lake sediments. J. Geophys. Res.: Biogeosci. 119, 1231–1243.
Stibal, M., et al., 2012. Methanogenic potential of Arctic and Antarctic subglacial environments with contrasting organic carbon sources. Glob. Change Biol. 18, 3332–3345.
Stuiver, M., Reimer, P.J., 1993. CALIB rev. 8. Radiocarbon 35, 215–230.
Teller, J.T., 1987. Proglacial Lakes and the Southern Margin of the Laurentide Ice Sheet.
Teller, J.T., Risberg, J., Matile, G., Zoltai, S., 2000. Postglacial history and paleoecology of Wampum, Manitoba, a former lagoon in the Lake Agassiz basin. Geol. Soc. Am. Bull. 112 (6), 943–958.
Teller, J.T., Leverington, D.W., 2004. Glacial Lake Agassiz: a 5000 yr history of change and its relationship to the δ18O record of Greenland. Geol. Soc. Am. Bull. 116, 729–742.
Teller, J.T., et al., 2008. Postglacial sedimentary record and history of west hawk lake crater, Manitoba. J. Paleolimnol. 40, 661–688.
Teodoru, C.R., et al., 2012. The net carbon footprint of a newly created boreal hydroelectric reservoir. Glob. Biogeochem. Cycles 26.
Thompson, H.A., White, J.R., Pratt, L.M., Sauer, P.E., 2016. Spatial variation in flux, $\delta^{13}C$ and $\delta^{2}H$ of methane in a small Arctic lake with fringing wetland in western Greenland. Biogeochemistry 131, 17–33.
Treat, C.C., Jones, M.C., Brosius, L., Grosse, G., Anthony, K.W., Frolking, S., 2021. The role of wetland expansion and successional processes in methane emissions from northern wetlands during the Holocene. Quat. Sci. Rev. 257, 106864.
Tweed, F.S., Carrivick, J.L., 2015. Deglaciation and proglacial lakes. Geol. Today 31, 96–102.
van Dongen, B.E., Semiletov, I., Weijers, J.W., Gustafsson, Ö., 2008. Contrasting lipid biomarker composition of terrestrial organic matter exported from across the Eurasian Arctic by the five great Russian Arctic rivers. Glob. Biogeochem. Cycles 22.
Vinšová, P., et al., 2022. The biogeochemical legacy of arctic subglacial sediments exposed by glacier retreat. Glob. Biogeochem. Cycles 36, e2021GB007126.
Wadham, J.L., Tranter, M., Tulaczyk, S., Sharp, M., 2008. Subglacial methanogenesis: a potential climatic amplifier? Glob. Biogeochem. Cycles 22, GB2021.
Wadham, J.L., et al., 2019. Ice sheets matter for the global carbon cycle. Nat. Commun. 10, 3567.
Waitt, Jr.R.B., 1980. About forty last-glacial Lake Missoula jökulhlaups through southern Washington. J. Geol. 88, 653–679.
Walter, K.M., Smith, L.C., Stuart Chapin, I.I.I.F., 2007. Methane bubbling from northern lakes: present and future contributions to the global methane budget. Phil. Trans. Royal Soc. A 365, 1657–1676.
Walter Anthony, K.M., Anthony, P., 2013. Constraining spatial variability of methane ebullition seeps in thermokarst lakes using point process models. J. Geophys. Res. Biogeosci. 118, 1015–1034.
Walter Anthony, K.M., Anthony, P., Grosse, G., Chanton, J., 2012. Geologic methane seeps along boundaries of Arctic permafrost thaw and melting glaciers. Nat. Geosci. 5, 419–426.
Walter Anthony, K.M., et al., 2021. Decadal-scale hotspot methane ebullition within lakes following abrupt permafrost thaw. Env. Res. Lett. 16, 035010.
Whiticar, M.J., 1999. Carbon and hydrogen isotope systematics of bacterial formation and oxidation of methane. Chem. Geol. 161, 291–314.
West, W.E., Creamer, K.P., Jones, S.E., 2016. Productivity and depth regulate lake contributions to atmospheric methane. Limnol. Oceanog. 61, S51–S61.
Williams, J.W., Shuman, B.N., Webb, T., Bartlein, P.J., Leduc, P.L., 2004. Late-quaternary vegetation dynamics in North America: scaling from taxa to biomes. Ecol. Monogr. 74, 309e334.
Yansa, C.H., Ashworth, A.C., 2005. Late pleistocene palaeoenvironments of the southern lake Agassiz basin, USA. J. Quat. Sci. 20, 255–267.
Young, N.E., Briner, J.P., 2015. Holocene evolution of the western Greenland Ice Sheet: assessing geophysical ice-sheet models with geological reconstructions of ice-margin change. Quat. Sci. Rev. 114, 1–17.
Young, J.M., Reyes, A.V., Froese, D.G., 2021. Assessing the ages of the Moorhead and Emerson phases of glacial Lake Agassiz and their temporal connection to the Younger Dryas cold reversal. Quat. Sci. Rev. 251, 106714.